National Library of Canada
Canadian Theses Service
Ottawa, Canada
K1A 0N4

Bibliothèque nationale du Canada
Services des thèses canadiennes

CANADIAN THESES

THÈSES CANADIENNES

NOTICE

The quality of this microfiche is heavily dependent upon the quality of the original thesis submitted for microfilming. Every effort has been made to ensure the highest quality of reproduction possible.

If pages are missing, contact the university which granted the degree.

Some pages may have indistinct print especially if the original pages were typed with a poor typewriter ribbon or if the university sent us an inferior photocopy.

Previously copyrighted materials (journal articles, published tests, etc.) are not filmed.

Reproduction in full or in part of this film is governed by the Canadian Copyright Act, R.S.C. 1970, c. C-30.

AVIS

La qualité de cette microfiche dépend grandement de la qualité de la thèse soumise au microfilmage. Nous avons tout fait pour assurer une qualité supérieure de reproduction.

S'il manque des pages, veuillez communiquer avec l'université qui a conféré le grade.

La qualité d'impression de certaines pages peut laisser à désirer, surtout si les pages originales ont été dactylographiées à l'aide d'un ruban usé ou si l'université nous a fait parvenir une photocopie de qualité inférieure.

Les documents qui font déjà l'objet d'un droit d'auteur (articles de revue, examens publiés, etc.) ne sont pas microfilmés.

La reproduction, même partielle, de ce microfilm est soumise à la Loi canadienne sur le droit d'auteur, SRC 1970, c. C-30.

THIS DISSERTATION HAS BEEN MICROFILMED EXACTLY AS RECEIVED

LA THÈSE A ÉTÉ MICROFILMÉE TELLE QUE NOUS L'AVONS REÇUE

NL-339 (r.86/06)

Canada

THE UNIVERSITY OF ALBERTA

The Effect of Mechanical Surface Modification on Fatigue in Relation to the Strain Hardening Rate of the Material

by

Douglas A. Rebinsky

A THESIS

SUBMITTED TO THE FACULTY OF GRADUATE STUDIES AND RESEARCH

IN PARTIAL FULFILLMENT OF THE REQUIREMENTS FOR THE DEGREE

OF MASTER OF SCIENCE

DEPARTMENT OF MECHANICAL ENGINEERING

EDMONTON, ALBERTA

SPRING 1986

Permission has been granted to the National Library of Canada to microfilm this thesis and to lend or sell copies of the film.

The author (copyright owner) has reserved other publication rights, and neither the thesis nor extensive extracts from it may be printed or otherwise reproduced without his/her written permission.

L'autorisation a été accordée à la Bibliothèque nationale du Canada de microfilmer cette thèse et de prêter ou de vendre des exemplaires du film.

L'auteur (titulaire du droit d'auteur) se réserve les autres droits de publication; ni la thèse ni de longs extraits de celle-ci ne doivent être imprimés ou autrement reproduits sans son autorisation écrite.

ISBN 0-315-30299-2

THE UNIVERSITY OF ALBERTA

RELEASE FORM

NAME OF AUTHOR Douglas A. Rebinsky

TITLE OF THESIS The Effect of Mechanical Surface Modification on Fatigue in Relation to the Strain Hardening Rate of the Material

DEGREE FOR WHICH THESIS WAS PRESENTED Master of Science

YEAR THIS DEGREE GRANTED Spring 1986

Permission is hereby granted to THE UNIVERSITY OF ALBERTA LIBRARY to reproduce single copies of this thesis and to lend or sell such copies for private, scholarly or scientific research purposes only.

The author reserves other publication rights, and neither the thesis nor extensive extracts from it may be printed or otherwise reproduced without the author's written permission.

(SIGNED) Douglas A. Rebinsky

PERMANENT ADDRESS:

8416- 135A Avenue

Edmonton, Alberta, Canada

T5E 1R6

DATED April 17, 1986

THE UNIVERSITY OF ALBERTA

FACULTY OF GRADUATE STUDIES AND RESEARCH

The undersigned certify that they have read, and recommend to the Faculty of Graduate Studies and Research, for acceptance, a thesis entitled "The Effect of Mechanical Surface Modification on Fatigue in Relation to the Strain Hardening Rate of the Material" submitted by Douglas A. Rebinsky in partial fulfilment of the requirements for the degree of Master of Science.

Supervisor

Date April 15, 1986

THE BROWN BERET

Abstract

The fatigue resistance of metal components may be improved by using the beneficial effects of mechanical surface modification. The scientific aspects of surface conditioning using surface rolling or shot peening have recently been scrutinized in order to optimize the attainable improvement of the properties.

A large number of variables influence the cold working of a metal near the surface; such as, the strain hardening characteristics of the material which may affect the depth of penetration and also, the magnitude and distribution of residual stresses. The present study is conducted to investigate these variables concerning surface rolling and fatigue life improvement.

Surface rolling was chosen as the surface conditioning process since the applied pressure can be closely monitored during the mechanical working of the surface of the part.

To consider extremes of strain hardening behavior, a HSLA steel (low rate of strain hardening and a high yield strength) and, after heattreating the HSLA steel, a dual phase steel (high rate of strain hardening and a low yield strength) were selected as model materials.

The theoretical and experimental results have indicated that there is a pronounced effect of the strain hardening characteristics on the penetration of work hardening. An increase in the rate of strain hardening will dramatically

increase the depth of plastic flow.

However, this does not necessarily influence the direct stress fatigue resistance.[4] The high rate of strain hardening of the dual phase steel substantially increased the depth of the work hardened zone when compared to that of the HSLA steel, but the direct stress fatigue strength at 10^7 cycles of the HSLA steel was improved twice as much as that of the dual phase steel. This may be explained by a shift in the location of fatigue crack initiation from the surface to within the core material. Therefore, an upper limit is achieved in improving by surface rolling the direct stress fatigue strength.

Acknowledgement

A number of people were instrumental in bringing this project to fruition. I am indebted to Dr. F. H. Vitovec for his guidance and helpful suggestions throughout this study. I would like to express my appreciation to the technical staff, especially the machinists, of the Mechanical Engineering Department for their assistance with many items in this investigation.

Also, I would like to thank my parents for their constant moral support during the past years of academic study consisting of the first day of my education to this Master's degree.

Table of Contents

Chapter Page

1. Introduction 1

1.1. Fatigue 1

1.1.1. Residual Stress 2

1.1.2. Surface Hardness 3

1.1.3. Surface Roughness 4

1.2. Effect of Strain Hardening on Several Parameters 5

2. Research Program 6

3. Experimental Procedure 8

3.1. Test Materials 8

3.2. Test Specimen 12

3.3. Surface Preparation 14

3.4. Testing Apparatus 18

3.5. X-Ray Stress Analysis 18

3.6. Microhardness 20

4. Results 22

4.1. Mechanical Properties of the Model Materials 22

4.2. Comparison of Surface Roughness 26

4.3. Depth of Penetration of Work Hardening 28

4.4. X-ray Surface Residual Stress Analysis 32

4.4.1. Theory of X-Ray Stress Analysis 32

4.4.2. Results of X-Ray Stress Analysis 36

4.4.2.1. Surface Residual Stress 36

4.4.2.2. Relaxation of Surface Residual Stress 39

4.5. Fatigue Properties of the Model Materials 42

5. Discussion 47

5.1. Modelling of Deformation Behavior 48

5.1.1. Empirical Equations 49

5.1.2. Law of Mixtures 56

5.1.3. Models based on Continuum Mechanics ... 57

5.1.3.1. Isostrain Condition 57

5.1.3.2. Strain Partitioning Condition .. 58

5.2. Theoretical Consideration of Indentation 61

5.2.1. The Problem of Indentation 61

5.2.1.1. Slip-Line Field Solution 62

5.2.1.2. Correlation of Theory with Experiment 65

5.2.2. Application of the Indentation Theory to the Results 70

5.2.2.1. Limit Theory 71

5.2.2.2. Effect of Strain Hardening on the Results 74

5.2.2.3. Hertz Theory 75

5.2.3. Summary of the Indentation Problem 77

5.3. Effect of Plastic Zone Depth on Residual Stress 77

5.4. Strain Hardening, Surface Rolling and Fatigue 84

6. Conclusions 89

References 90

Appendix A : Elastic-Plastic Bending of a Beam 99

Appendix B : Fatigue Life Data 103

List of Tables

Table	Description	Page
1	Comparison of Mechanical Properties.	24
2	Comparison of Surface Residual Stress.	38
3	Comparison of Fatigue Properties.	45

List of Figures

Figure	Description	Page
1	Microstructure of the Thermomechanically Treated High Strength Low Alloy Steel.	9
2	Microstructure of the Dual Phase Steel heattreated at 730°C, water quenched.	9
3	Schematic Diagram of the Tensile Behavior of the HSLA and Dual Phase Steels.	10
4	Process of Intercritical Annealing.	11
5	Shape of the Amsler Test Specimen.	13
6	Spring Loaded Surface Roller Mechanism.	17
7	The Surface Rolling Process.	17
8	Comparison of the Engineering Stress-Strain Curves for the Various Test Materials.	23
9	Comparison of Surface Roughness.	27
10	Penetration of Surface Rolling as determined by Microhardness using a Vickers Indenter.	30
11	Depth of Penetration of Work Hardening as determined by Fry's Reagent Etching.	31
12	Schematic Diagram of a Debye-Scherrer Ring.	33
13	Comparison of the Diffraction Rings for Different Surface Conditions.	37
14	Cyclic Loading Induced Relaxation of the Surface Residual Stresses within the Surface Rolled HSLA Steel.	40
15	Cyclic Loading Induced Relaxation of the Surface Residual Stresses within the Surface Rolled Dual Phase Steel.	41
16	Effect of Surface Rolling on Fatigue Strength.	43
17	Comparison of the Flow Stress Properties using Hollomon's Method of Analysis.	51
18	Crussard-Jaoul Analysis.	53
19	Comparison of the Strain Hardening Characteristics of the Various Steels.	55

20	Mileiko's Theory of Composites compared to the Test Materials.	59
21	The Stress System in Plane Plastic Flow.	64
22	Plane Strain Slip-Line Field for a Blunt Indenter.	66
23	Plastic Zone for a Strain Hardening Material produced by Blunt Indentation.	66
24	A Limit Theory Statically Admissable Stress Field for a Plane Strain Blunt Indenter.	73
25	A Limit Theory Velocity Field for a Plane Strain Blunt Indenter.	73
26	Comparison of Experimental Data of the Relaxation of the Longitudinal Surface Residual Stress with an Empirical Equation for the HSLA Steel.	81
27	Comparison of Experimental Data of the Relaxation of the Longitudinal Surface Residual Stress with an Empirical Equation for the Dual Phase Steel.	82
28	Comparison of the Fatigue Failure Fracture Surfaces of the Surface Rolled Dual Phase and HSLA Steels.	86
A1	Cross-Section and Stress Distribution of an Elastic-Plastic Circular Section in Bending.	100

Nomenclature

φ	Angle turned by either a α or β slip-line
F	Applied Force
γ	Austenite
η	Bisection Angle concerning Diffraction
a	Contact Half-width or Radius
θ	Diffraction Angle
$K\alpha_1$	Diffraction Ring
R	Diffraction Ring Radii
D	Distance from Specimen to Film
e	Engineering Strain
S	Engineering Stress
α	Ferrite
P	Hydrostatic Pressure
ψ_o	Incidence Angle
d	Lattice Plane Spacing
E	Modulus of Elasticity
N	Number of Cycles
ν	Poisson's Ratio
τ	Shear Stress
n	Strain Hardening Exponent
ϵ_p	True Plastic Strain
ϵ	True Strain
σ	True Stress
Y	Yield Strength
HV	Vickers Hardness

1. Introduction

The beneficial effects of mechanical surface modification of metal parts by shot-peening or surface rolling to improve the fatigue strength of a component have been known and exploited for some time [1-4]. However, recently there has been renewed interest, particularly in the scientific aspects of this surface-conditioning process, to optimize the attainable improvement of several technological parameters [4-13]. Specifically, the main factors which influence the fatigue strength of a material are metallurgical, mechanical and geometric effects. These include: state of material, depth of plastic deformation from the surface-conditioning process, residual stresses and surface preparation.

1.1. Fatigue

The failure mode described as metal fatigue is caused by reverse plastic deformation for both nucleation and propagation of a crack. In general, metal fatigue is a surface sensitive phenomenon. This is explained by a reduced constraint on the grains near the surface which induces those grains near the surface to yield at a lower applied stress than those in the bulk [14, 15, 16]. Therefore, the fatigue strength of a metal part can be improved by reducing the applied stress near the surface by

the introduction of residual stresses [1, 2, 4-13, 17, 18]. Also, an increase of the yield strength of the surface material will improve the fatigue strength. This is achieved by surface hardening; such as, cold working by shot-peening or surface rolling. Thus, these processes provide a favorable residual stress distribution along with an increase in the yield strength near the surface to aid in the improvement of the fatigue strength of the metal part [14, 19].

1.1.1. Residual Stress

During the mechanical processing of a metal part, local plastic deformation occurs resulting in a residual stress distribution. The magnitude and distribution of residual stresses is related to the deformation process [20, 21]. In this situation, the procedure of modifying the surface through mechanical working, either shot-peening or surface rolling, creates a compressive residual stress pattern at the surface [1, 2, 4, 20-22].

These residual stresses arise when the applied pressure causes local plastic deformation along the surface. Since the mechanical working of the surface by shot-peening or surface rolling produces an expansion of the deformed zone, the interior must restrain this stretched region to satisfy compatibility. Hence, when the external stress is removed, the plastically deformed zone prevents the adjacent elastic

regions from recovering to the previously unstrained state. An equilibrium condition results within the material through the restraint of the plastically deformed zone by a residual compressive stress state created by the elastically stretched interior which remains in residual tension [2, 20-23].

The significance of these residual stresses in affecting the fatigue behavior of a material depends upon: their magnitude and orientation, their relaxation, the modulus of elasticity and the yield strength of the material, and the range of applied stress [7, 8, 12-15, 17, 19, 24]. These must be considered in evaluating the improvement of the fatigue strength of a metal component.

1.1.2. Surface Hardness

The mechanical working of the surface by shot-peening or surface rolling not only creates compressive residual stresses, but it also strain-hardens the surface to some depth of penetration dependent on the applied load and the properties of the material. Strain hardening can be simply defined as an increase in yield strength due to some increment in plastic deformation of the material [23, 26, 27].

An increase in hardness or yield strength of the surface layer will enable it to withstand a larger applied load than previously. This increase offsets the lower constraint within the surface layer. Therefore, an increase in surface

strength will require a larger applied cyclic load to induce local plastic deformation since there is an increase in the requirement to yield the surface. Thus, the fatigue strength should show an improvement due to a hardened surface [8, 9, 11, 14, 19, 24]. Also, there is an upper limit to the amount of improvement in fatigue strength to be gained from increasing the hardness of the surface. Since the location of crack initiation can shift to the inside of this hardened layer, the "strength" of the base material again becomes important in evaluating the fatigue strength of the mechanically worked component [7, 28, 29].

Hence, the effect of strain hardening on the depth of penetration of the hardened layer also will play an important role in the improvement of fatigue strength.

1.1.3. Surface Roughness

The roughness of a surface provides a qualitative estimate of the amount of crack nuclei available for initiation and later propagation of a fatigue failure under cyclic loading [14]. An increase in surface roughness provides an increase in the sharpness and depth of cavities and asperities which produce a strain concentration. To decrease the roughness, the surface can be mechanically worked by shot-peening or surface rolling to not only provide cold working and strain hardening in the surface layer, but also, drastically reduce the large-scale

roughness to a much improved surface condition where the asperities are considerably flattened. Thus, there is a smaller tendency for premature initiation of a crack to produce failure of a component.

Therefore, the surface condition should be included in a study of the fatigue strength of a material [14, 19].

1.2. Effect of Strain Hardening on Several Parameters

Strain hardening characteristics may also affect the relaxation of the compressive residual stress state within this cold worked region during cyclic loading [14, 15, 25].

Hence, an accurate examination of the influence of mechanical surface modification must take into consideration not only the state, magnitude, orientation and relaxation under cyclic loading of the induced compressive residual stresses, but it must also include the increase of strength of the metal in the deformed zone along with the effect of strain hardening characteristics of the material on all the parameters of concern.

2. Research Program

The objective of this study is to investigate the influence of strain hardening characteristics on the effectiveness of mechanical surface modification for improvement of the fatigue strength.

First, the study required two materials of vastly different strain hardening characteristics. As model materials, structural steels, stainless steels, cast irons and others can be used. For this project, a high strength low alloy (HSLA) steel was used whose strain hardening characteristics could be altered by heat treating in the dual phase region. Hence, the composition of the two model materials is the same with only a change in their microstructure.

A HSLA steel and, upon re-heat treatment, a dual phase steel were selected for a variety of different reasons: they show extremes of strain hardening which can be changed by heattreatment, they are the result of recent development, their specific properties are not as yet fully explained and they are readily available.

Cold working by surface rolling rather than shot-peening was chosen because the geometry of interaction and the contact pressure can be closely controlled with this method.

Thus, with the two model materials and the method of mechanical surface modification chosen, a research program

can be outlined.

Several parameters were required to be determined: the strain hardening characteristics of each material, the penetration of cold working resulting from surface rolling, the magnitude of the initial plus the cyclically relaxed surface residual stresses by x-ray diffraction stress analysis techniques, the difference in surface roughness between polished and surface rolled specimens, and most importantly the respective fatigue life responses to reversed direct tension-compression cyclic loading.

3. Experimental Procedure

3.1. Test Materials

As a model material with a low strain hardening rate, a high strength low alloy (HSLA) steel from Kawasaki Steel Corporation was chosen with the following weight percent alloy composition: 0.10 C, 1.55 Mn, 0.014 P, 0.006 S, 0.27 Si, 0.040 Nb, 0.035 V and 0.034 Al. The small alloy additions of vanadium and niobium provide strength through grain refinement and the production of precipitates. Also, the HSLA steel was processed by a thermomechanical treatment which is temperature controlled rolling. This produces a state similiar to cold working while retaining a fine grain size. In Figure 1, the resultant microstructure is shown which is basically composed of ferrite and pearlite with a ferrite grain size of ASTM 12.5 [30]. The thermomechanical treatment produces a high yield strength and a low strain hardening rate shown schematically in Figure 3. Thus, these steels are difficult to form.

To improve formability, a new method of heat treating has been introduced which results in a low yield strength and a high strain hardening rate (Figure 3) [31-35]. This is achieved by "intercritical annealing" (Figure 4) of the steel to produce a "dual phase" structure consisting of ferrite and martensite (Figure 2) [31, 32, 36]. Basically, the steel is heated to a temperature within the

Figure 1 : Microstructure of the Thermomechanically Treated High Strength Low Alloy Steel. (Magnification : 1000 x)

Figure 2 : Microstructure of the Dual Phase Steel heattreated at 730°C, water quenched. (Magnification : 1000 x)

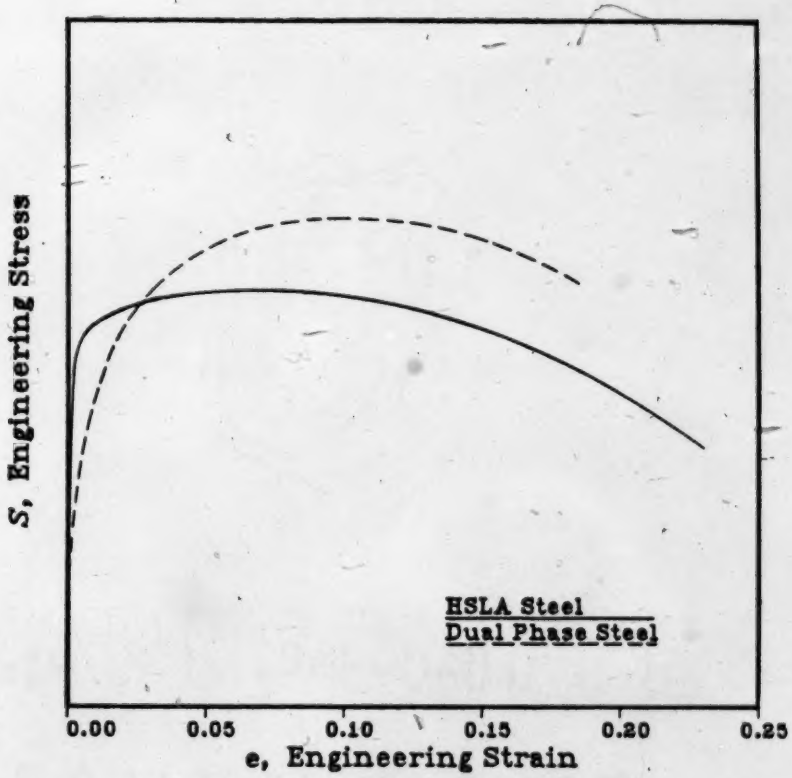

Figure 3 : Schematic Diagram of the Tensile Behavior of the HSLA and Dual Phase Steels.

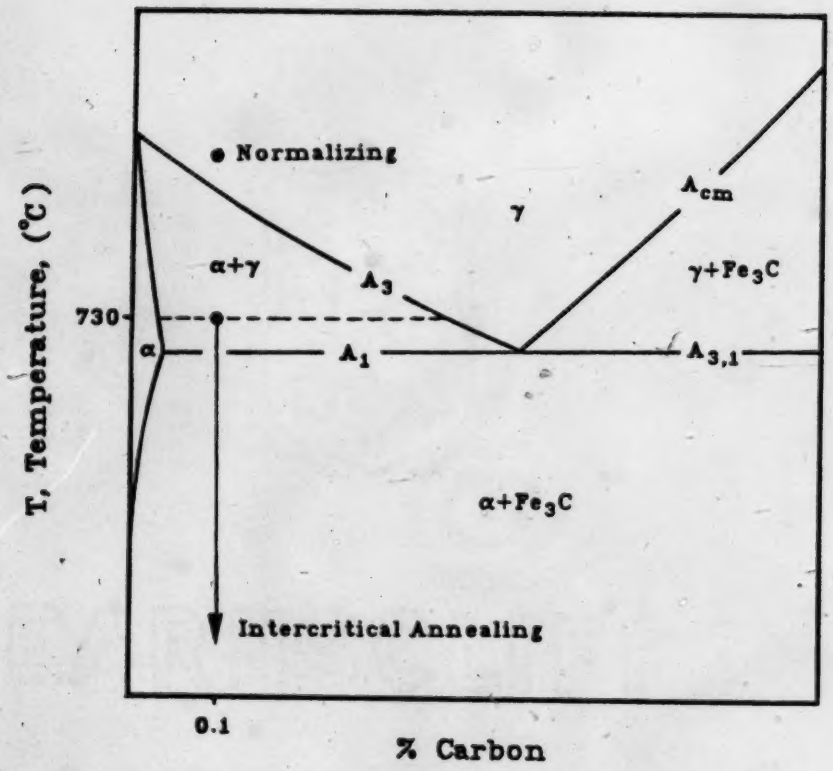

Figure 4 : Process of Intercritical Annealing.

two phase ferrite and austenite zone of the phase diagram and then quenched causing the austenite to transform into martensite within a ferrite matrix [31, 32]. By varying the amount of carbon and the intercritical annealing temperature of the steel, a dual phase steel with different strengths and strain hardening characteristics can be produced. Also, the yield strength of the HSLA steel is achieved by the dual phase steel after 2 to 3% deformation (Figure 3). This is the frequent degree of deformation for some automobile forming operations [35].

Therefore, the model materials chosen have very different strain hardening characteristics:

1. the HSLA steel with a high yield strength and low strain hardening rate,
2. and re-heat treating the HSLA steel to form a dual phase steel with a low yield strength and high strain hardening rate.

3.2. Test Specimen

The shape of the test specimen was of Amsler design with a 8 mm diameter and a gauge length of 30 mm (Figure 5).

To summarize the test condition of the HSLA steel, test specimens were cut from the as received pipe section longitudinally to the rolling direction. The prior deformation of the material was from pipe forming and expansion. This amounts to approximately 4% total strain

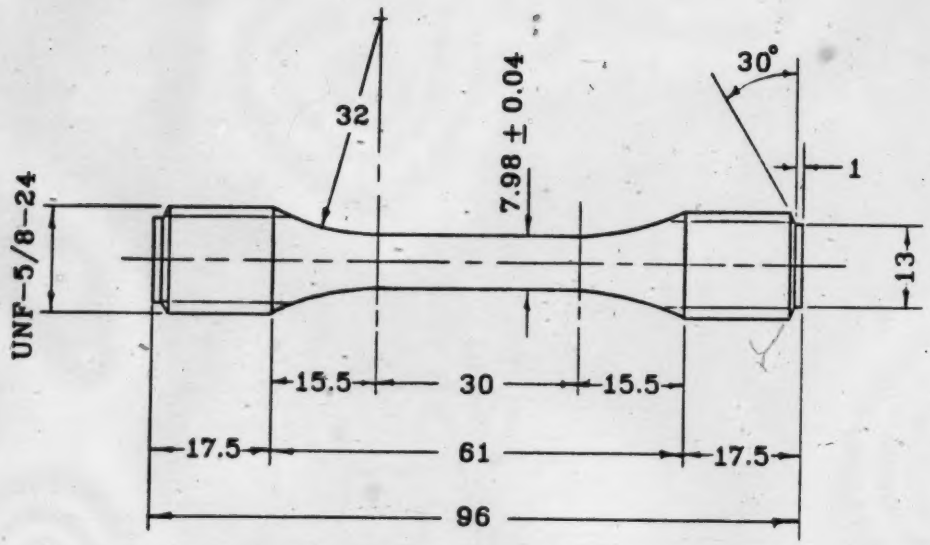

All measurements in millimeters except thread size.

Figure 5 : Shape of the Amsler Test Specimen.

plus natural aging for six years at an ambient temperature of 20 °C.

For the dual phase steel, the above mentioned HSLA steel was first normalized at 900 °C for 0.5 hour followed by air cooling. Then, test specimens were machined to the shape shown in Figure 5. After machining, the normalized test specimens were intercritically annealed in a reducing atmosphere at 730 °C for 0.5 hour followed by an abrupt water quench to form the ferrite-martensite microstructure. The volume percent of martensite from areal analysis was about 25%.

3.3. Surface Preparation

After the machining procedure stated in section 3.2., the HSLA steel and normalized specimens were mechanically polished with 600 grit emery paper. Next, the normalized steel specimens were intercritically annealed as per the procedure previously stated. Some oxidation did occur and the heavy blue oxide layer was removed by mechanical polishing using 240 grit paper.

All the specimens were electrolytically polished in a chromic acid solution within a cylindrical concentric copper cathode [37]. The chromic acid solution contains 1 L of phosphoric acid and 9.5 g of chromium trioxide. The polishing procedure for all the specimens was 14 minutes at 4 volts (approximately 6 amps) followed by 6 minutes at

2.5 volts (approximately 2 amps) with the chromic acid being slightly agitated by a stirring bar at 500 rpm at a solution temperature of 90 °C.

The rate of solution at 4 volts was approximately 0.120 mm/h compared to 0.056 mm/h at 2.5 volts. The predicted amount of radial removal was 0.038 mm; whereas, the measured value was 0.025 mm. This small discrepancy is probably due to the inaccuracy of measurement.

At this depth of etching, the effects of cold work due to machining were considered negligible. Since the grain size of the steel was about ASTM 12.5 which corresponds to an average grain size of 0.0047 mm [30] and the total amount removed radially was 0.025 mm, 5.3 grain diameters were removed by electrolytic polishing. From the literature, the average depth of plastic deformation by machining of a low carbon steel varies from 0.025 to 0.050 mm [38, 39]. These penetrations were determined by observing at what depth the residual stress was 75% of the surface value. The work hardened depth created by machining is highly dependent upon the material and the machining parameters used [39]. Extrapolating these values to this study, the average plastic flow depth of machining may be estimated to be within 5 to 10 grain diameters. Therefore, a significant amount of the cold worked layer is considered to be removed by the electrolytic polishing procedure.

It is important to consider the depth of cold working produced by machining and the amount removed by electrolytic

polishing since this work hardened region may effect the magnitude and distribution of residual stresses introduced by surface rolling [4].

Approximately half of the HSLA and dual phase steel specimens were surface rolled to introduce compressive residual stresses and work harden the surface layer. This was accomplished using a mirror polished, hard roller of 28.6 mm (1.125 in.) diameter with a contour radius of 3.2 mm (0.125 in.), shown in Figure 6, compared to an approximate specimen diameter of 8 mm (0.315 in.). A roller load of 178 N (40 lb_f) with a specimen speed of 160 rpm and a feed rate of 0.173 mm/turn (0.0068 in./turn) was chosen along with a coverage corresponding to six passes. Also, the surface velocity of the specimen was 67 mm/s (2.6 in/s).

At first, only one roller was used for cold working the surface. This produced acceptable results in the HSLA steel but, upon cold working of the dual phase steel, the test specimen was observed to deflect approximately 0.064 mm (0.0025 in.) at the center compared to less than 0.025 mm (0.0010 in.) for the HSLA steel. This large deflection in the dual phase steel may change the magnitude and orientation of the residual stresses as compared to a constrained surface rolling process. The bending of the test specimen due to surface rolling using one roller was analyzed considering elastic-plastic beam theory and it is shown in Appendix A that the surface begins to yield when

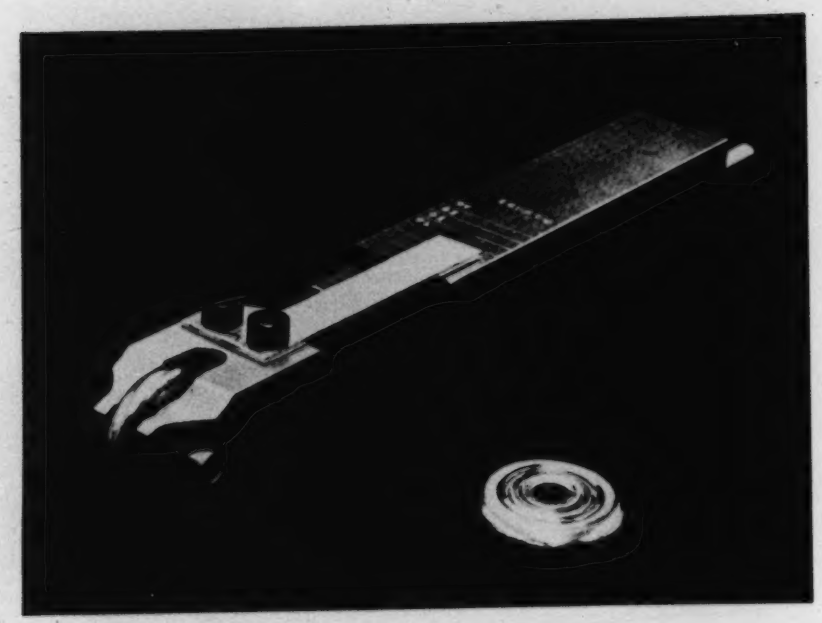

Figure 6 : Spring Loaded Surface Roller Mechanism.

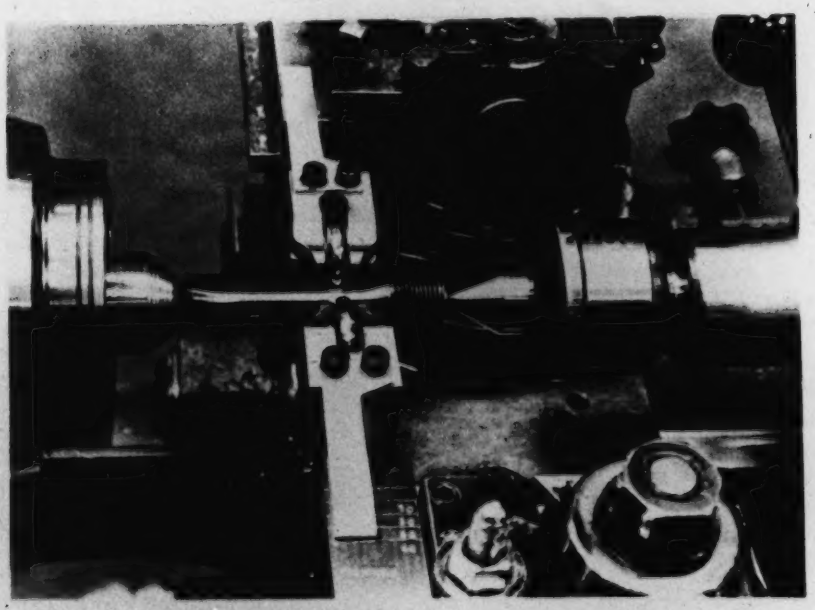

Figure 7 : The Surface Rolling Process.

the deflection is equal to the experimentally determined value of 0.064 mm (0.0025 in.) [40-43]. Therefore, it was decided to use two rollers placed on opposite sides of the test specimen (Figure 7) to eliminate the deflection. This also will increase the overall amount of cold working. As mentioned previously for one roller, the same parameters in the surface rolling process are used for two rollers.

3.4. Testing Apparatus

The tensile tests and reversed stress fatigue tests were performed on a MTS Resonant Servo-Hydraulic Testing Facility with a load capacity of $\pm$650 kN ($\pm$146000 lb_f).

The mechanical properties of the HSLA and dual phase steels were examined through tension tests using stroke control with a ramp of approximately 0.01 mm/s. The loads and displacements were digitally recorded using a personal computer (IBM PC) with an analog/digital converter board (Metrabyte) at a rate of 4 ordered pair values a second. Each value was the average of 20 loads or displacements.

The fully reversed direct stress tension-compression fatigue tests were cycled at a frequency of 10 Hertz in load control to failure.

3.5. X-Ray Stress Analysis

Residual stresses were determined in the longitudinal

and circumferential directions for the various types of test specimen condition: machined, polished and surface rolled for both model materials [44-46]. Also, the relaxation of these surface residual stresses due to fatigue loading was measured at several intervals during the reversed stress cyclic loading test. This comprised of the removal of the test specimen from the fatigue testing machine to perform x-ray diffraction photography in a separate apparatus. After completion of the x-ray analysis, the test specimen was then placed back with the previous orientation into the testing machine and cycled to the next interval. It is important to maintain the same orientation of the test specimen within the testing apparatus to reduce of the effect of eccentricity of loading. Also, care was taken not to shock load the test specimen during placement and removal from the fatigue testing machine.

An x-ray generator (Siemens Kristalloflex 2H) along with a flat camera to absorb and photograph the diffracted x-ray beam from the steel test specimen was used [44-46]. The entrance diaphram used to collimate the x-ray beam had a cross-section of 0.8 mm x 1.6 mm.

Chromium radiation was used with x-ray generator settings of 50 kV and 20 mA. The exposure time was approximately 10 minutes to produce a significantly intense $K\alpha_1$ diffraction ring from the (211) lattice plane spacing of the steel specimen. This corresponded to a diffraction angle, θ of 78.04°. It was not necessary to use a $K\beta$ filter

since the $K\alpha_1$ peak was well defined and readily recognized by the microdensitometer (Joyce, Loebl and Co. Ltd.) used to scan the intensity peaks of the diffraction ring on the exposed film.

A computer program was then used to calculate the stress from several microdensitometer scans of the exposed film. The final results were the mean of several values. The erroneous points were removed from the set by the use of Chauvenet's criterion for small sample sizes. Simply, the calculated stresses which were ± 2 standard deviations from the sample mean were removed from the set and then the mean was recalculated.

3.6. Microhardness

A Leitz microhardness tester was used with a Vickers indenter and a 50 g load to determine the depth of penetration due to surface rolling [47, 48, 49]. Measurements were made transverse to the specimen axis to a depth of 0.4 mm (0.015 in.) at 0.025 mm (0.001 in.) intervals. The final values used were the average of at least eight indentations at every interval, or a total of approximately 200 microhardness readings per curve. The indentations were carefully spaced so that no interference would occur between them.

The HSLA steel specimens were mounted in bakelite at 150 °C using a Buehler mounting apparatus, then polished to

a final grit of 0.05 μm. The dual phase steel specimens were slowly cut on a Buehler Low Speed saw with a diamond impregnated blade to avoid cold working during cutting. Then, they were etched in a 2% Nital solution to remove any cold work created during sawing. Lastly, they were carefully polished with minimal applied pressure and a 0.05 μm gamma alumina grit [50].

The difference in preparation procedure is due to the extreme strain hardening characteristics of the dual phase steel. If the same procedure was used as with the HSLA steel, severe work hardening from sawing, polishing and aging due to bakelite mounting would have increased the microhardness above the actual value for the dual phase steel [49].

4. Results

In the previously discussed experimental procedure, several tests were outlined to analyze a specific variable concerning the study of fatigue strength improvement by mechanical surface modification as influenced by the strain hardening characteristics of the material. These variables include the mechanical properties of the material, depth of penetration of strain hardening, magnitude and relaxation of residual stresses, and the surface roughness of each test specimen condition.

4.1. Mechanical Properties of the Model Materials

The engineering stress-strain curves of the HSLA and dual phase steels are shown in Figure 8. Several important parameters are summarized in Table 1 which describe in an approximate manner the shape and magnitude of the engineering stress-strain curve for each specific material. These parameters are the yield strength at 0.2% offset, the ultimate tensile strength, the uniform elongation, the total elongation and the reduction of area.

The yield strength defined at 0.2% offset for the HSLA steel is about 40% greater than that of the dual phase steel for both polished and surface rolled conditions. At 2% offset, which is about the amount of plastic deformation in some forming processes [35], the flow stress of all the

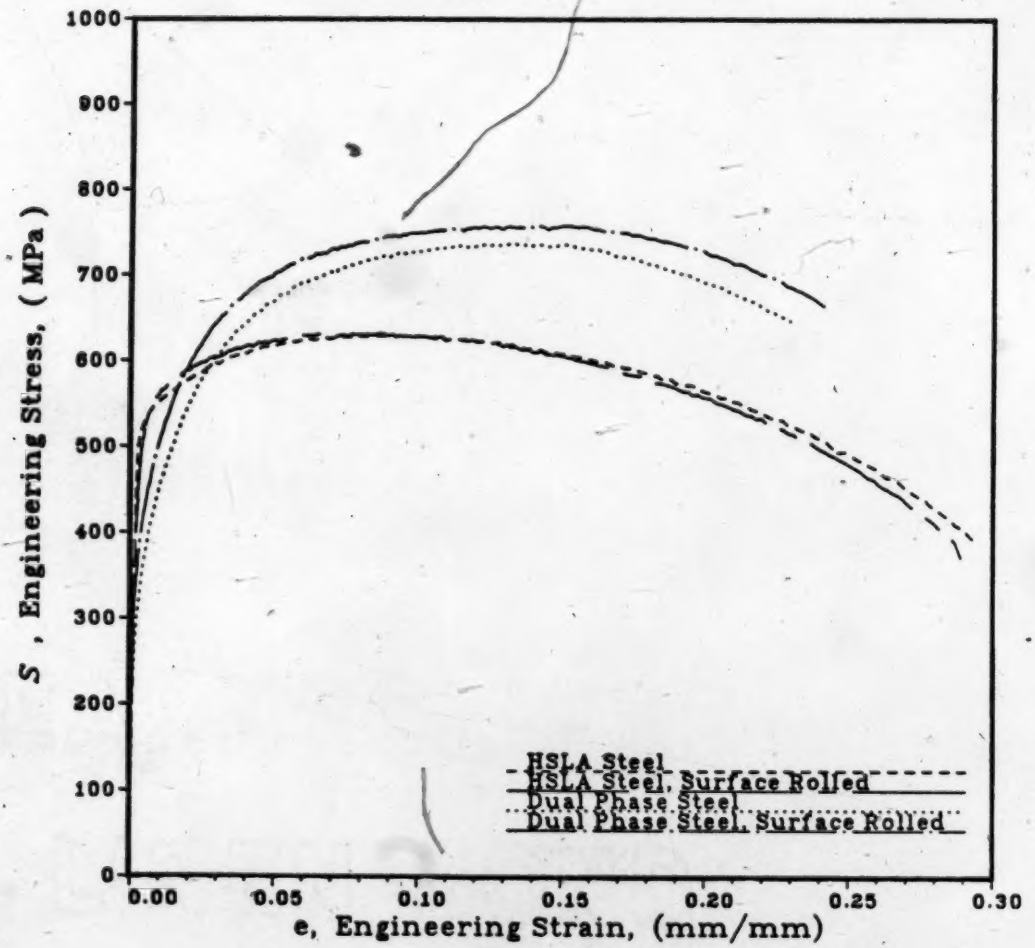

Figure 8 : Comparison of the Engineering Stress–Strain Curves for the Various Test Materials.

Table 1 : Comparison of Mechanical Properties.

Material	0.2% Offset Yield Strength (MPa)	0.2% Offset Flow Stress (MPa)	Ultimate Tensile Strength (MPa)	Ultimate Elongation (%)	Total Elongation (%)	Reduction of Area (%)
HSLA Steel	515	580	631	9.5	29.2	69.6
HSLA Steel, Surface Rolled	495	590	631	8.1	28.8	71.0
Dual Phase Steel	353	587	740	13.5	22.8	43.2
Dual Phase Steel, Surface Rolled	375	621	757	13.1	24.0	36.9

materials is approximately the same corresponding to a value around 590 MPa. Therefore, after plastically deforming the dual phase steel, it will have the same "strength" as the HSLA steel.

Comparing the ratio of the yield strength at 0.2% offset to the ultimate tensile strength for each of the model materials, one observes that the HSLA steel has reached 80% of its tensile strength within 0.2% elongation; thus, little capacity is left for further work hardening at larger degrees of plastic deformation. The dual phase steel is able to work harden to a greater extent since it is only stressed to 50% of its tensile strength at that amount of elongation.

The total elongation of the HSLA steel in either condition is approximately 20% larger than that of the dual phase steel. Also, the reduction of area is about 40% greater for the HSLA steel. But, the uniform elongation of the HSLA steel is 30% smaller than that of the dual phase steel.

Thus, although the HSLA steel will deform plastically to a much larger extent considering ductility, it will surpass the ultimate tensile strength much earlier than the dual phase steel. Therefore, it is actually in some ways weaker due to the possible formation of a triaxial state of stress followed by plastic instability. The metal part or component at this deformed state can no longer support the required load.

4.2. Comparison of Surface Roughness

The surface roughness in terms of a centerline average using a K cut-off for the HSLA steel in machined, polished and surface rolled conditions are 0.16 μm, 0.13 μm and 0.28 μm respectively. For the dual phase steel, the centerline average surface roughness using K cut-off is 0.24 μm for a polished surface compared to 0.22 μm for the surface rolled condition.

In Figure 9, the above states of surface condition for the two model materials are compared to facilitate observation of the various different types of roughness over some finite length of the test specimen. The scales are magnified approximately 100 X in the horizontal direction and about 15000 X in the vertical direction.

Upon comparison of these centerline average surface roughness values and the longitudinal surface sample scans, the test specimen surface condition can be observed and analyzed considering the random texture and waviness.

The height and sharpness of the asperities are drastically reduced when the HSLA steel machined test specimen is electrolytically polished. When the HSLA steel test specimen is surface rolled, all sharp asperities and cavities are eliminated [51] and the roughness basically corresponds to a waviness produced by the roller mechanism. For the dual phase steel, the increase in roughness above the machined state after electrolytic polishing may be due

a). HSLA Steel, Machined

b). HSLA Steel, Polished

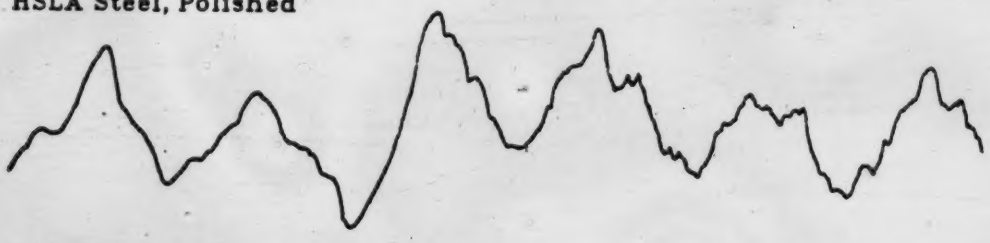

c). HSLA Steel, Surface Rolled

d). Dual Phase Steel, Polished

e). Dual Phase Steel, Surface Rolled

Figure 9 : Comparison of Surface Roughness.
(Magnification : Horizontal = 100 x, Vertical = 15000 x)

to the preferential attack of the martensite by the chromic acid polishing solution. As previously commented for the surface rolled condition, the dual phase steel roughness again corresponds to a waviness with negligible sharp cavities and asperities.

The amplitude of the waviness for the surface rolled dual phase steel, 0.22 μm, is smaller when compared to the corresponding, 0.28 μm, for the HSLA steel. This lowering in the amplitude of the waviness can be attributed to the lower yield strength and higher work hardening rate of the dual phase steel. Thus, in a simplified analysis, the amount of upward flow of deformed material around the indenter, or roller, is less for the dual phase steel in comparison to the HSLA steel [23].

From the above discussion, the change from short wavelength roughness, with sharp asperities and cavities, to large wavelength roughness will significantly decrease the amount of strain concentration at the surface. Thus, this will increase to some degree the fatigue life of the material [51].

4.3. Depth of Penetration of Work Hardening

The penetration of work hardening produced by surface rolling was measured using two methods. First, the Vickers microhardness was determined from the surface to some depth at intervals transverse to the specimen axis. These results

are shown in Figure 10. The surface rolling penetration for the HSLA steel was approximately 0.33 mm compared to 0.57 mm for the dual phase steel. The criterion used to estimate these penetration depths for work hardening was the intersection of the surface rolled microhardness data described by a polynomial curve fit with the average value base material curve which was increased by 1% to provide a definite meeting point of the two curves. This was done to accommodate the asymptotic behavior concerning the decrease with depth of microhardness produced by surface rolling.

The work hardened depth was also determined using Fry's reagent [52] to etch a finely polished transverse cut slice from the surface rolled model materials. Photographs of these work hardened rings using bright field illumination are shown in Figure 11. The HSLA steel penetration depth of surface rolling is about 0.32 mm compared to 0.25 mm for the dual phase steel.

Upon comparison of the hardness and etching methods, the penetrations for the HSLA steel are equal, but the dual phase steel result differs by 56%. The requirement to successfully use Fry's reagent is that the steel be in an aged condition in order for the plastically deformed zone to become visible after etching. This may decrease the width of the ring, which provides an estimate of penetration depth, for the dual phase steel. The surface rolled dual phase steel test specimen in this case was aged at 150 °C for 15 minutes during bakelite mounting. The plastically

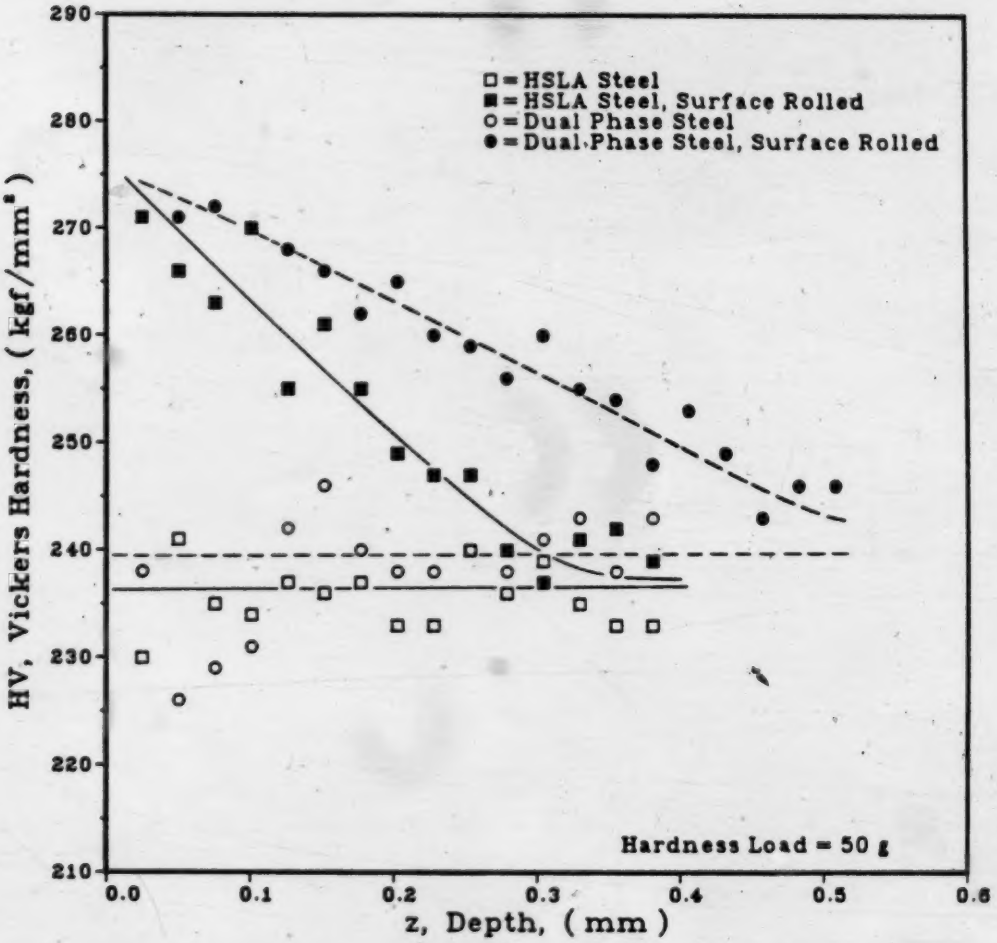

Figure 10: Penetration of Surface Rolling as determined by Microhardness using a Vickers Indenter.

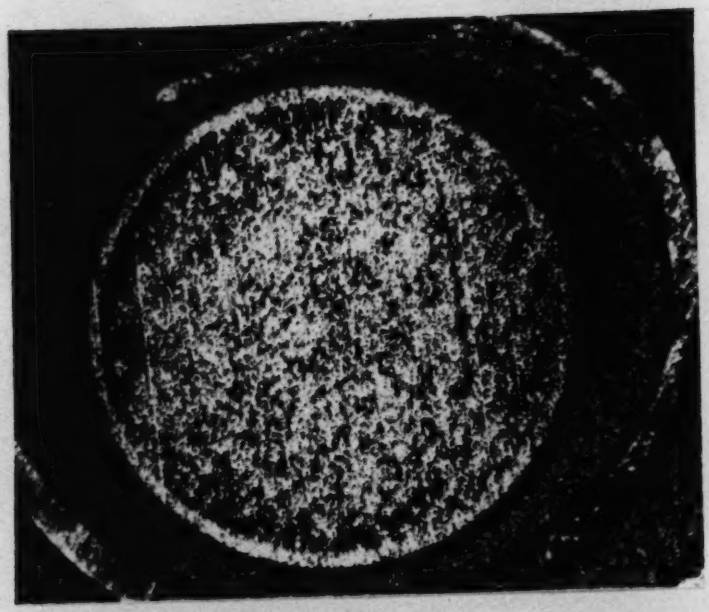

a). HSLA Steel, Surface Rolled

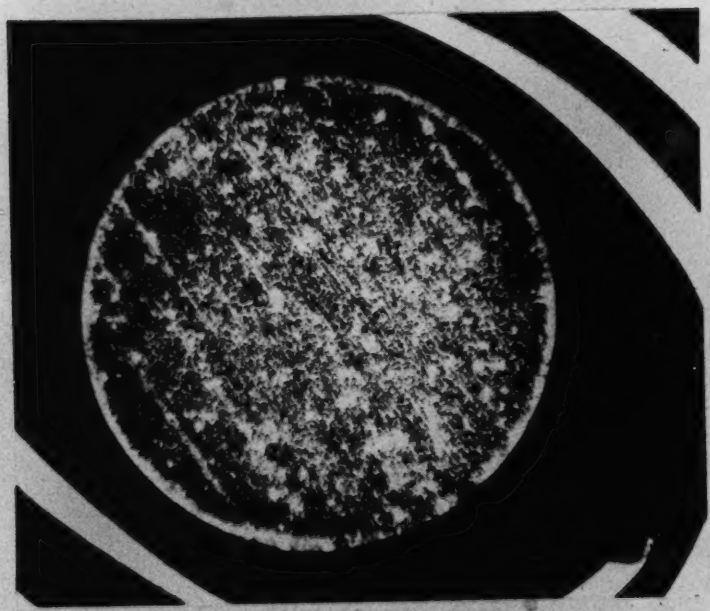

b). Dual Phase Steel, Surface Rolled

Figure 11 : Depth of Penetration of Work Hardening as determined by Fry's Reagent Etching. (Magnification : 9.5 x)

deformed zone and base material may react differently to this aging causing different changes in the yield strength within these two regions of the dual phase steel test specimen [53]. Thus, when etched with Fry's reagent, a different ring thickness is observed than may exist in the original state. Also, the etchant may not perform to the same extent or efficiency on the dual phase steel as compared to the HSLA steel.

4.4. X-Ray Surface Residual Stress Analysis

4.4.1. Theory of X-Ray Stress Analysis

A non-destructive method of measuring the surface residual stress is x-ray diffraction which relates the stress to the distortion of the atomic lattice. Upon deformation of a material, the interplanar crystal spacings, d, increase or decrease depending on the orientation of the applied loading. The amount of change in interplanar spacing is a measure of the residual stress [45, 54, 55, 56, 57].

In Figure 12, the Debye-Scherrer ring due to the diffracted collimated x-ray beam is shown. Also, it can be observed that the closely collimated beam hits the surface of the test specimen obliquely and produces an egg-shaped ring on the film which absorbs the back scatter. From, this ring eccentricity, the size of the internal stress can be

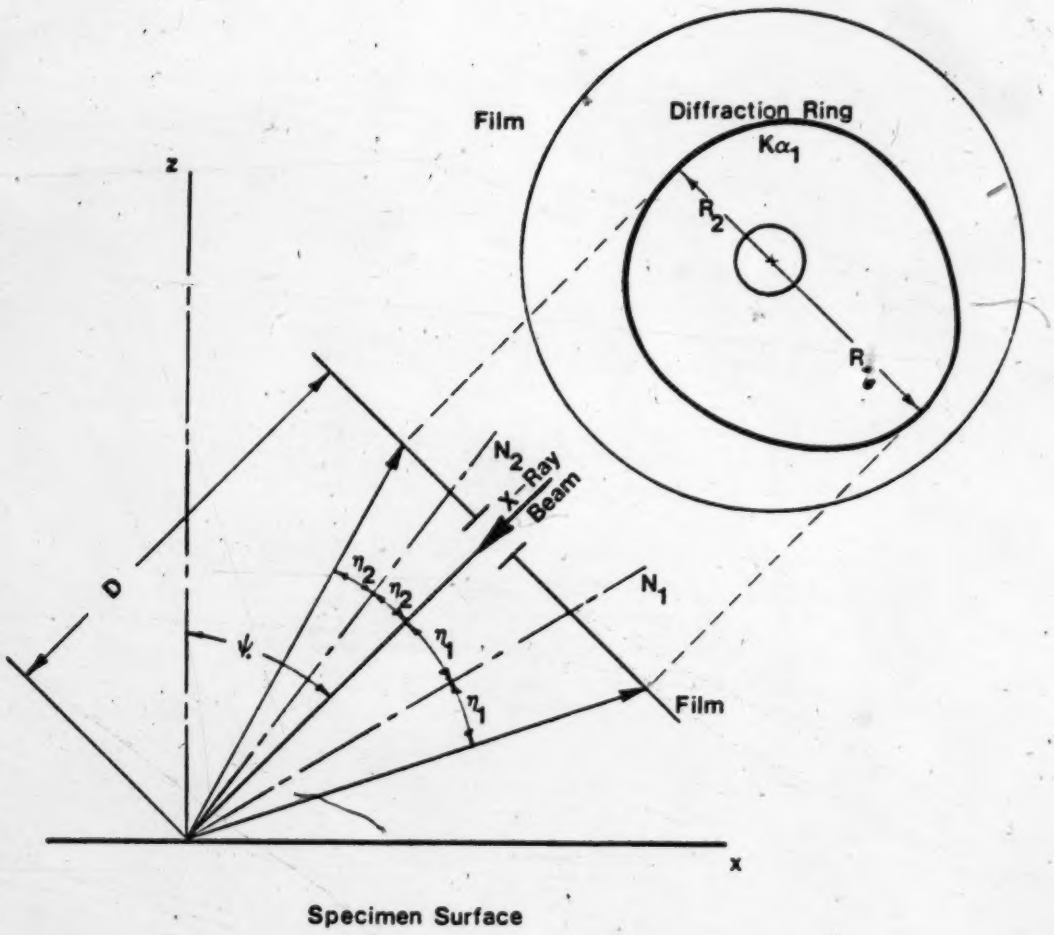

Figure 12 : Schematic Diagram of a Debye–Scherrer Ring [54–56].

determined.

Actually, the Debye-Scherrer ring eccentricity is related to the elongation of the material. This elongation is then converted into a stress by using Hooke's law. In this study, it was assumed that the elastic constants consisting of the modulus of elasticity, E and Poisson's ratio, ν do not vary between mechanical and radiographic studies. The effect of anisotropy of the test materials was neglected.

Applying the theory of elasticity, an equation is obtained which relates the stress in some direction to the difference in elongation. Next, the lattice plane spacing can be related to the difference in elongation. Combining these two relations, this final equation can be further simplified by substituting an incidence angle, ψ_o of 45° and for the single exposure method one obtains;

$$\sigma = \frac{d_1 - d_2}{d_1} \frac{E}{1 + \nu} \frac{1}{\sin \eta} \qquad (1)$$

where η is the average of η_1 and η_2 which are the bisection angles concerning the position of the Debye-Scherrer ring with the incidence angle. By using the Bragg law and geometry, a relationship is obtained between the lattice plane spacing and the difference in radii from the Debye-Scherrer ring on the exposed film;

$$\Delta R = 2D \sec^2 2\theta \tan \theta \frac{\Delta d}{d} \qquad (2)$$

where θ is the diffraction angle and D, the distance from

the radiated steel specimen to the film [54-56]. Therefore, the residual stress can be calculated from the exposed film by using a microdensitometer to determine ΔR.

The error in the calculated longitudinal residual stress using the single exposure method described above was estimated from a mathematical error analysis as 50 MPa. This is comparable with values stated in the literature which ranged from 35 to 70 MPa [54, 55]. The error in the circumferential residual stress is about 20% larger due to alignment problems in achieving the 45° incidence angle since the test specimen had a small radius. Thus, a small change in the x-ray beam position will change the incidence angle, ψ_o significantly from the 45° assumed value in the derivation of equation (1).

To determine whether the stress is tensile or compressive, the film cassette is rotated 180° and a second exposure is made on the unexposed opposite half of the film. If the more densely blackened reflection is further outside the lighter ring, the stress is compressive; otherwise, the stress is tensile [45].

In addition to these measured and calculated macroresidual stresses, the amount of microresidual stresses can be approximated from the width of the Debye-Scherrer ring. A widening of the ring shows more microresidual stresses are contained in the material. This is a qualitative estimate of the variance in stress between grains due to induced plastic deformation.

4.4.2. Results of X-Ray Stress Analysis

4.4.2.1. Surface Residual Stresses

Several Debye-Scherrer rings are shown in Figure 13. One can observe that in the polished condition of both model materials, HSLA and dual phase steels, the internal stress is approximately zero for the longitudinal direction. In the dual phase steel photograph, individual spots appear within the interference ring. This shows that the dual phase steel in this state is virtually free of microresidual stresses.

After surface rolling of the two materials, there is a considerable amount of eccentricity in the diffraction ring. Therefore, a large compressive macroresidual stress exists within the surface layer of both materials. Also, the amount of microresidual stresses has increased greatly as shown by the considerable widening of the Debye-Scherrer ring.

In Table 2, the results of the surface residual stress x-ray analysis are compared as to machined, polished and surface rolled conditions for both model materials (HSLA and dual phase steels).

In all situations, the circumferential stress is slightly larger than the longitudinal stress except for the polished HSLA steel. This shows that the circumferential stress penetrates the specimen to a greater extent than the

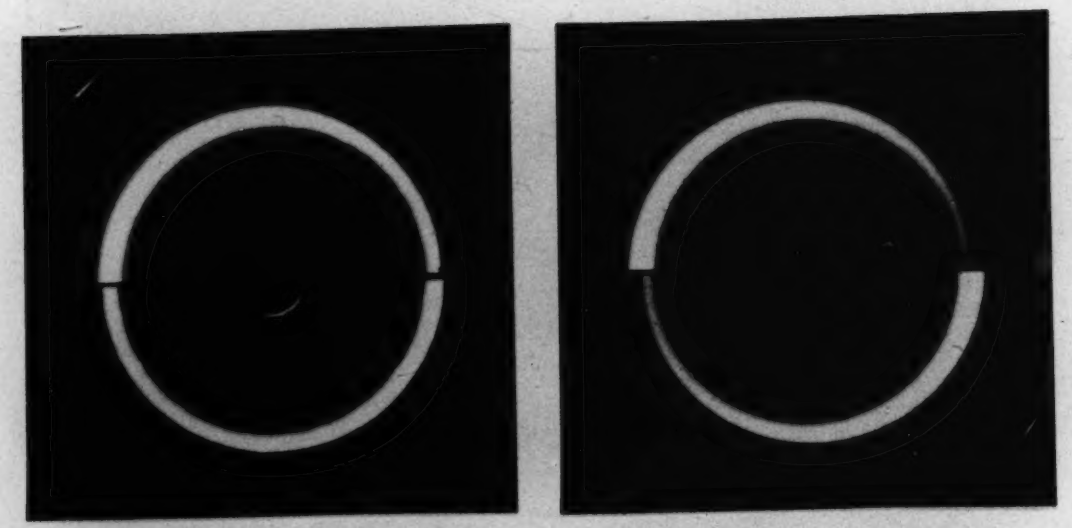

a). HSLA Steel, Polished

b). HSLA Steel, Surface Rolled

c). Dual Phase Steel, Polished

d). Dual Phase Steel, Surface Rolled

Figure 13 : Comparison of the Diffraction Rings for Different Surface Conditions.

Table 2 : Comparison of Surface Residual Stress.

Material	Surface Condition		
	Machined*	Polished*	Surface Rolled*
HSLA Steel (Longitudinal)	-546	-99	-629
HSLA Steel (Circumferential)	-573	-560	-644
Dual Phase Steel (Longitudinal)	---	-107	-670
Dual Phase Steel (Circumferential)	---	-96	-682

*All Residual Stress values in MPa

longitudinal stress during machining. The difference in longitudinal and circumferential stress for the surface rolled condition is due to the shape of the roller which produces an elliptic shaped indentation with the Hertz theory predicting the circumferential stress to be about 1.1 times larger than the longitudinal stress. Experimentally, the ratio is about 1.02 which is within the analysis errors.

Next, the surface rolled dual phase steel surface residual stresses are slightly larger than the values obtained for the HSLA steel. This is probably due to the higher potential for work hardening of the dual phase steel.

4.4.2.2. Relaxation of Surface Residual Stress

In Figures 14 and 15, the relaxation induced by cyclic loading is shown for the surface rolled HSLA and dual phase steels respectively.

Comparison of the results for the two materials can only be qualitative, since the applied cyclic load in each situation was not equal. Although, for both materials, the applied cyclic load did correspond to their respective fatigue strengths at 10^7 cycles.

The longitudinal surface residual stress for the HSLA steel decays rapidly in the first 10 cycles. It is approximately reduced to half the original value. Whereas, the dual phase steel's longitudinal surface residual stress does not start to relax until the application of 100 loading

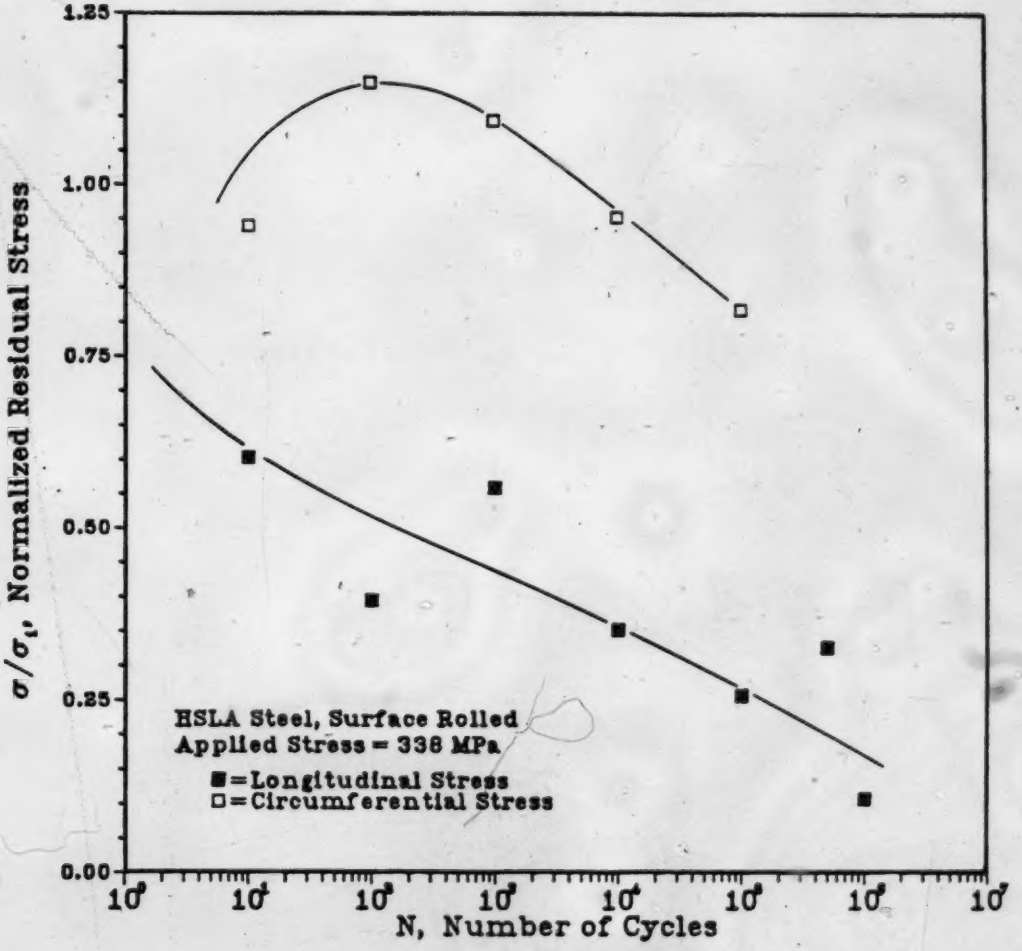

Figure 14: Cyclic Loading Induced Relaxation of the Surface Residual Stresses within the Surface Rolled HSLA Steel.

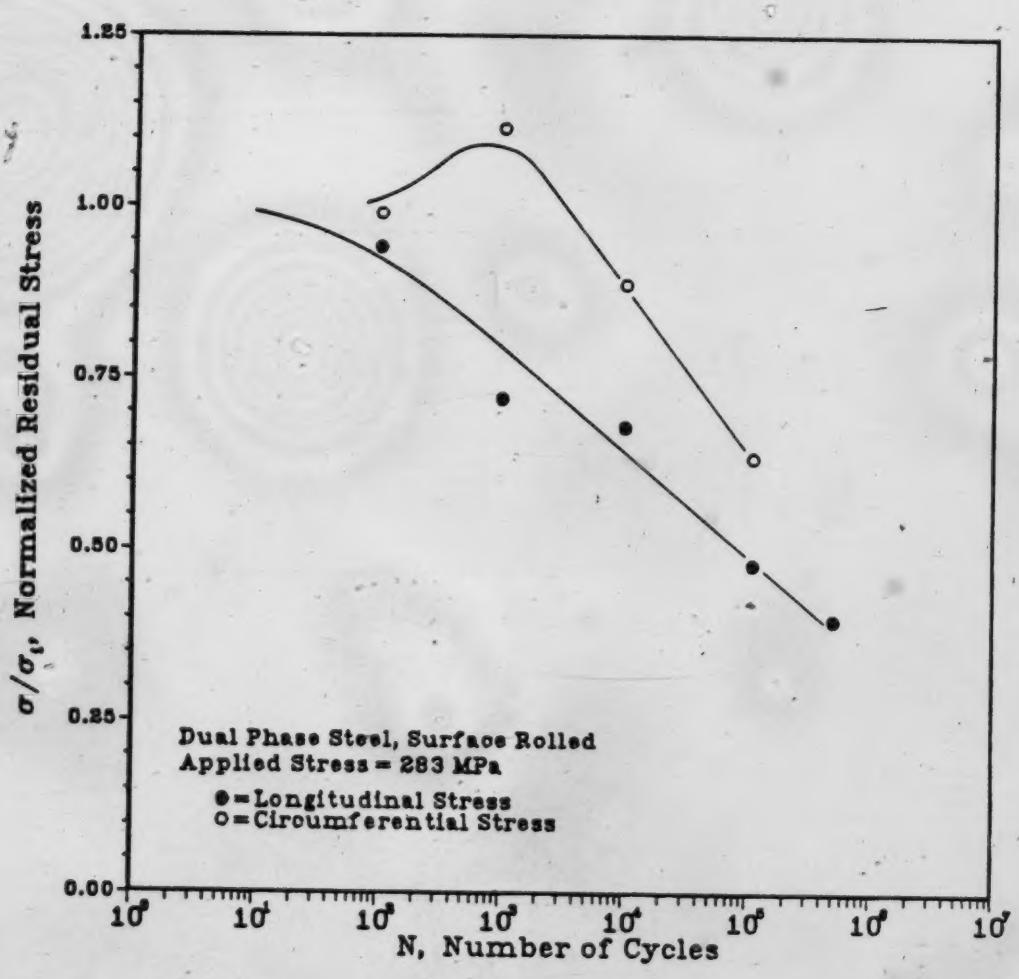

Figure 15: Cyclic Loading Induced Relaxation of the Surface Residual Stresses within the Surface Rolled Dual Phase Steel.

cycles. Thus, the effect of a larger depth of penetration of plastic deformation due to surface rolling is observed to promote greater stability of the surface residual stresses in the dual phase steel [25]. After 10^2 cycles, the relaxation rate of the longitudinal surface residual stress for the dual phase steel is greater than that of the HSLA steel. But, the longitudinal surface residual stress for the dual phase steel was always larger in magnitude when compared to the HSLA steel.

For the surface rolled HSLA steel, the circumferential surface residual stress increases for some time followed by a relaxation rate equal to the longitudinal stress relaxation rate. This increase in compressive residual stress due to cyclic loading followed by decay has been observed previously [58]. In comparison, the surface rolled dual phase steel circumferential surface residual stress decays at a faster rate than the longitudinal stress after 10^3 cycles.

The major observation is that the longitudinal compressive residual stress of the surface rolled dual phase steel does not relax as quickly when compared to the surface rolled HSLA steel.

4.5. Fatigue Properties of the Model Materials

The results of the fully reversed direct stress (tension-compression) fatigue tests are shown in Figure 16

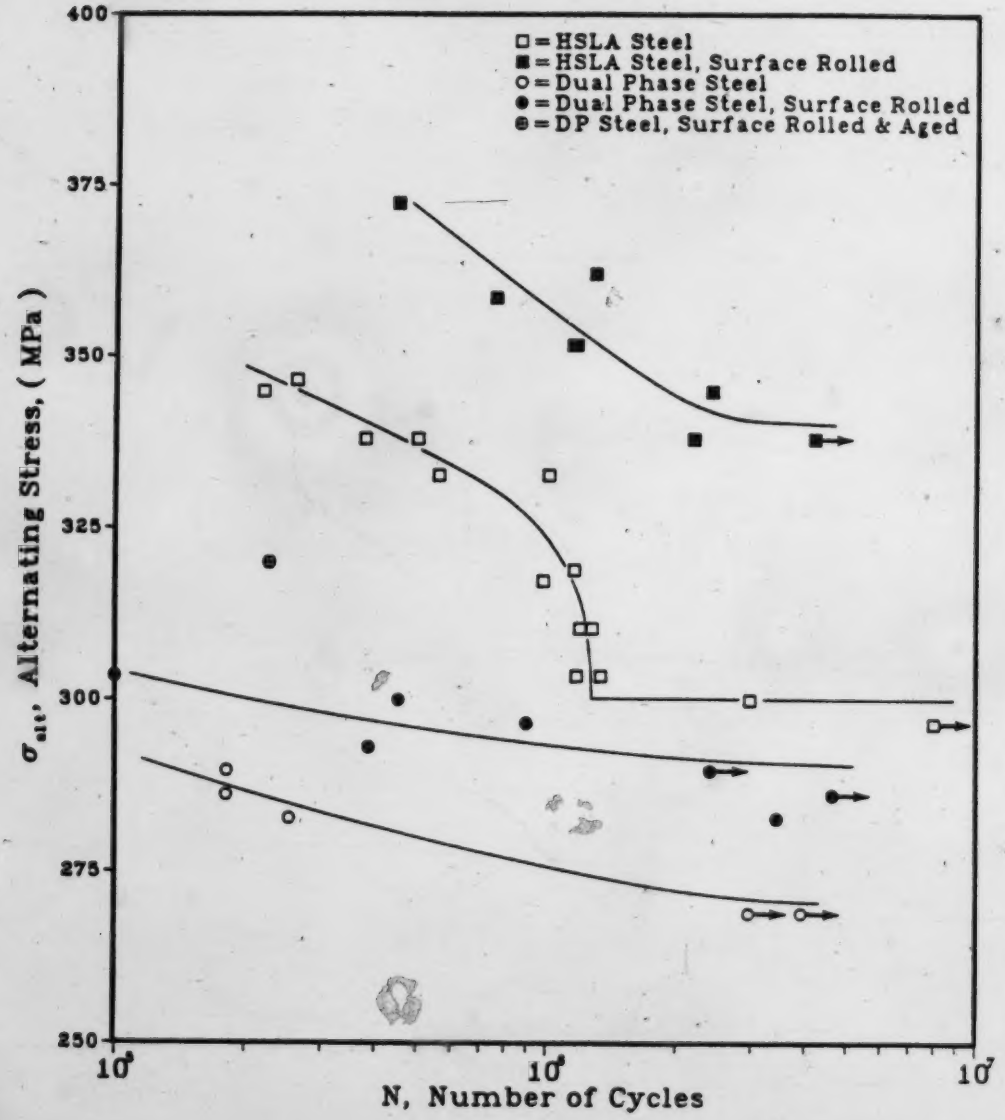

Figure 16: Effect of Surface Rolling on Fatigue Strength.

and Appendix B. The fatigue strengths defined at 10^7 cycles of the HSLA and dual phase steels in both polished and surface rolled conditions are compared in Table 3.

From Figure 16, it is observed that the polished and surface rolled dual phase steel fatigue curves are very flat. Thus, a small increase in applied stress will produce a drastic decrease in life of the component. The HSLA steel will require a much larger increase in applied stress to reduce the fatigue life to the same extent as with the dual phase steel.

The surface rolling procedure provides a 13% improvement in the fatigue strength at 10^7 cycles for the HSLA steel; whereas, the dual phase steel improves only by 7%. Thus, the fatigue strength improvement at 10^7 cycles due to surface rolling of the HSLA steel is about twice that of the dual phase steel.

In comparing the fatigue strengths at 10^7 cycles, the polished dual phase steel value is 9% lower than the polished HSLA steel. After surface rolling the dual phase steel, the fatigue strength is still 3% lower when compared to the polished HSLA steel.

Next, when a surface rolled dual phase steel specimen is aged at 180 °C for 30 minutes and cyclically loaded, the fatigue strength is substantially increased but it still does not achieve the fatigue strength of the HSLA steel as shown in Figure 16. The HSLA steel fatigue life at 320 MPa is approximately 4 times longer in comparison to the aged

Table 3 : Comparison of Fatigue Properties.

Material	Fatigue Strength at 10^7 cycles (MPa)	Ratio of Fatigue Strength to Ultimate Tensile Strength	Ratio of Fatigue Strength to 0.2% Offset Yield Strength
HSLA Steel	300	0.48	0.58
HSLA Steel, Surface Rolled	340	0.54	0.69
Dual Phase Steel	272	0.37	0.77
Dual Phase Steel, Surface Rolled	292	0.39	0.78

surface rolled dual phase steel.

Therefore, a preliminary statement is that the axial loading fatigue properties of the HSLA steel in polished and surface rolled conditions are superior to that of the dual phase steel in either of the states in this study. The effect of surface rolling may be different if stress gradients are introduced during cyclic loading; such as, those which occur in bending or torsion fatigue.

5. Discussion

In order to evaluate the effect of strain hardening on on surface rolling to improve the fatigue strength, an understanding of the plastic flow behavior is required of the two model materials. From this analysis, the model materials may then be mathematically described to aid in the explanation of indentation, or surface rolling, of materials with different work hardening properties.

For this purpose, the literature was surveyed to obtain various models and analytical approaches pertinent to this study [59-95]. These mathematical formulations are briefly reviewed to examine and state their features and limitations. It appears that the analytical solutions to this problem have not sufficiently matured for a rigorous analysis which would provide information on the penetration of plastic deformation as a function of non-linear strain hardening. Without rigorous models or concepts to describe the effect of strain hardening characteristics on the depth of plastic flow, the magnitude and distribution of the resulting residual stresses from the indenting process can only be estimated along with the influence of stress cycling on cyclic hardening or softening and the relaxation of these residual stresses.

The detailed survey only enabled the application of a qualitative analysis to describe the previously stated variables. This qualitative analysis has indicated that

there is a pronounced effect of the strain hardening characteristics on the penetration of cold work due to surface rolling. However, this does not necessarily influence the fatigue resistance produced by work hardening the surface.

5.1. Modelling of Deformation Behavior

To describe the deformation behavior of materials, a tensile test is usually performed to obtain an engineering stress-strain curve. This is a graph of the applied tensile load divided by the original area plotted as a function of the percent elongation measured over some specified gage length [23]. For the model materials used in this study, these curves are shown in Figure 16 of section 4.1. These curves do not quantitatively characterize the strain hardening ability of a material [59]. A mathematical model is required to investigate the strain hardening characteristics of the material in a more rigorous manner.

The engineering stress-strain curve is based on the original dimensions of the specimen. Since these dimensions change continuously during the test, this curve does not provide a true indication of the deformation characteristics of a material. A better description of the plastic flow behavior of a material is obtained by measuring the stress and strain instantaneously. The relationship produced using instantaneous results is called the true stress-true strain

curve. This provides an improved method of examining the instantaneous plastic deformation of a material.

The past methods of approximating material behavior at high strains include: elastic-perfectly plastic or elastic-linear work hardening models. Neither of these models is applicable to the dual phase steel. A representation is required that will provide for continuous work hardening which is observed in the true stress-true strain curve of the dual phase steel.

Several attempts have been made to represent the continuous work hardening of some materials, which include dual phase steels, with either empirical relationships and/or equations derived from continuum mechanics. These expressions can then be used to mathematically compare the strain hardening characteristics of the two model materials. Also, it may provide an accurate interpretation of the different responses of these materials to some applied mechanical process.

5.1.1. Empirical Equations

First, an empirical equation based on the true stress-true strain curve can be applied to the two model materials to describe their tensile properties. A simple relationship is the Ludwik equation [23],

$$\sigma = \sigma_o + K\varepsilon_p^{\,n} \qquad (3)$$

which describes some power curve relation to the plastic deformation after some yield point stress, σ_o. A better fit is obtained for the HSLA and dual phase steels by using the Hollomon equation [59],

$$\sigma = K\varepsilon_p^{\,n} \qquad (4)$$

where n is the strain hardening exponent and K is the strength coefficient. These coefficients can be determined by two methods of analysis which use the true stress-strain curves of the materials [31, 60-64]. The analysis was performed numerically using a computer program and the previously mentioned digitally recorded load-displacement tensile data.

The first method is to plot the logarithm of the true flow stress as a function of the logarithm of the true plastic strain. This produces a linear relationship as shown by;

$$\log \sigma = \log K + n \cdot \log \varepsilon_p \,. \qquad (5)$$

For the HSLA and dual phase steels, the logarithmic true stress-true plastic strain curves are shown in Figure 17. An observation from examining these curves is that the dual phase steel's flow stress is increasing at a much greater rate than the HSLA steel. Thus, it exhibits a higher degree of work hardening. Also, for all the test materials, the relationship is not linear but it is described in a piecewise linear manner by several different slopes or

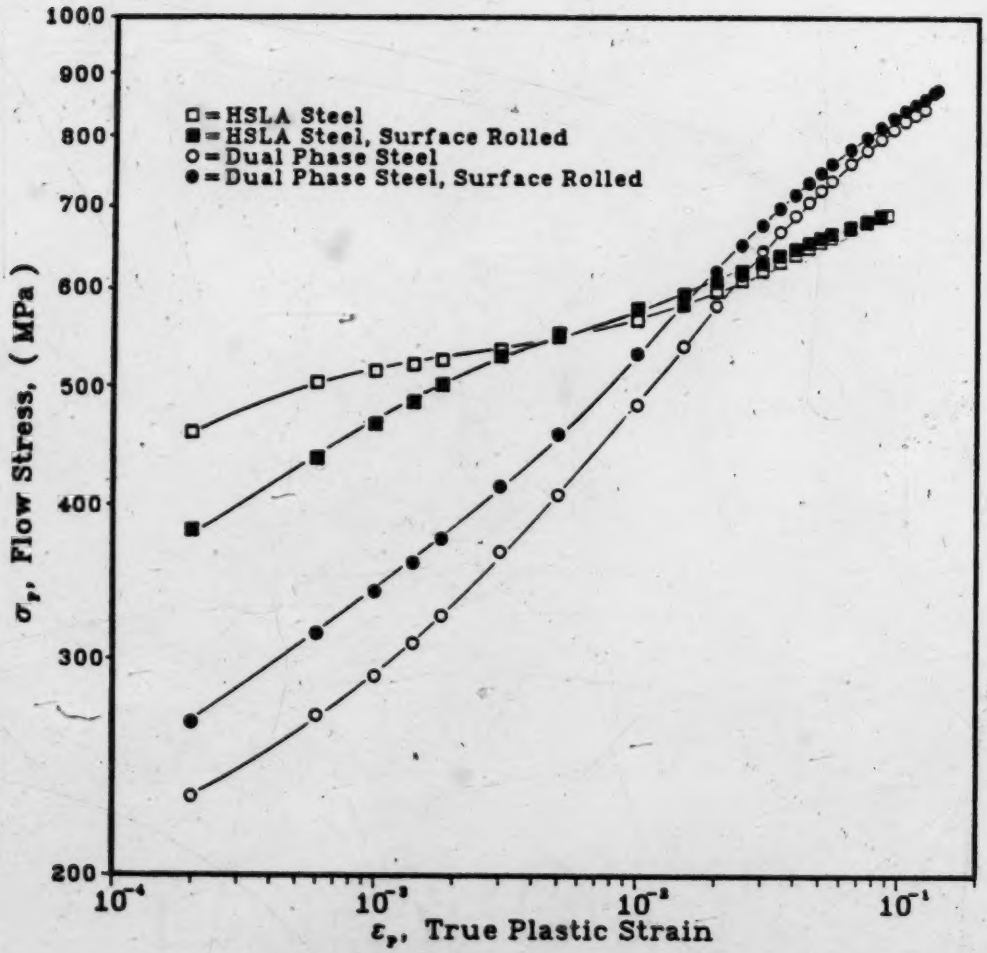

Figure 17: Comparison of the Flow Stress Properties using Hollomon's Method of Analysis.

strain hardening exponents. This response has been previously observed [31, 62-64]. The change in slope of this curve may indicate different mechanisms of strain hardening [31]. Therefore, a single power curve equation cannot adequately represent the work hardening characteristics of the HSLA and the dual phase steels.

Also, from Figure 17, the overall effect of the surface rolling procedure has strengthened or work hardened the dual phase steel; whereas, it has decreased the flow stress at small strains in the HSLA steel. This may be attributed to the introduction of residual stresses and a work hardened surface layer.

Another procedure which can be applied to determine the coefficients in the Hollomon or Ludwik equations is the method devised by Crussard and Jaoul [60, 61, 64]. This involves the logarithm of the derivative of equations (4) and (5);

$$\log \frac{d\sigma}{d\varepsilon_p} = \log nK + (n-1) \cdot \log \varepsilon_p \ . \qquad (6)$$

This method was applied to the HSLA and dual phase steels used in this study (Figure 18). Again, the strain hardening exponent is observed to be a function of the true plastic strain.

Thus, the strain hardening component can be determined as a function of the true flow stress and the true plastic strain as given by [23];

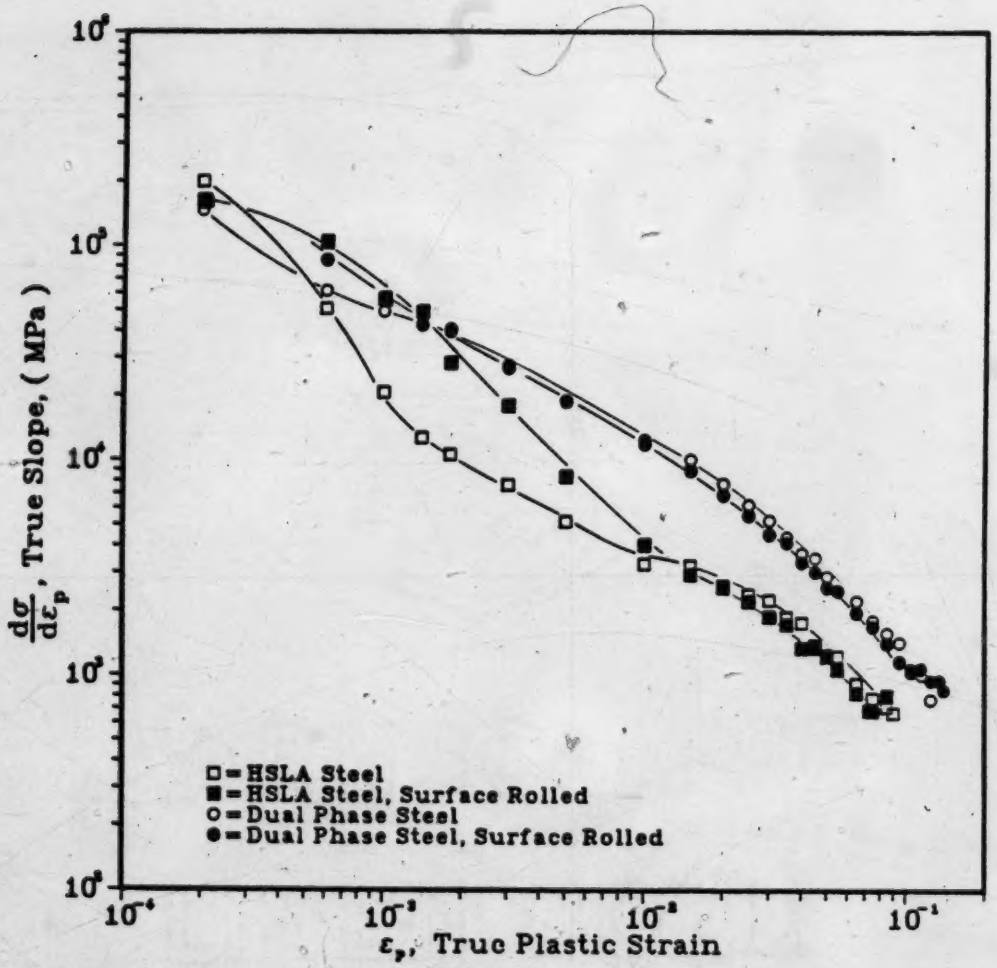

Figure 18: Crussard–Jaoul Analysis.

$$n = \frac{\varepsilon_p}{\sigma} \frac{d\sigma}{d\varepsilon_p} \qquad (7)$$

where the true slope and the strain hardening exponent, n were calculated numerically with a computer program using a three point differentiation scheme. With this method of describing the strain hardening characteristics of the model materials, a better overall picture is obtained of the plastic flow characteristics of the materials being studied. The HSLA and dual phase steels' strain hardening abilities are compared in this manner in Figure 19. The dual phase steel in both conditions work hardens to a much greater extent than the HSLA steel. At a true plastic strain of 0.02, the strain hardening exponent of the dual phase steel is three times that of the HSLA steel. Even at the uniform strain of both materials, this coefficient for the dual phase steel is still approximately twice that of the HSLA steel.

The largest difference in strain hardening between the two materials is observed to occur for plastic strains smaller than 0.03. Recall that this is the usual extent of deformation in some automobile forming operations [35]. Hence, the dual phase steel is work hardening extensively during mechanical processing in comparison to the negligible amount of work hardening taking place in the HSLA steel.

Generally, the surface rolling procedure decreases the available amount of strain hardening for both materials (Figures 17 and 19). Although at true plastic strains

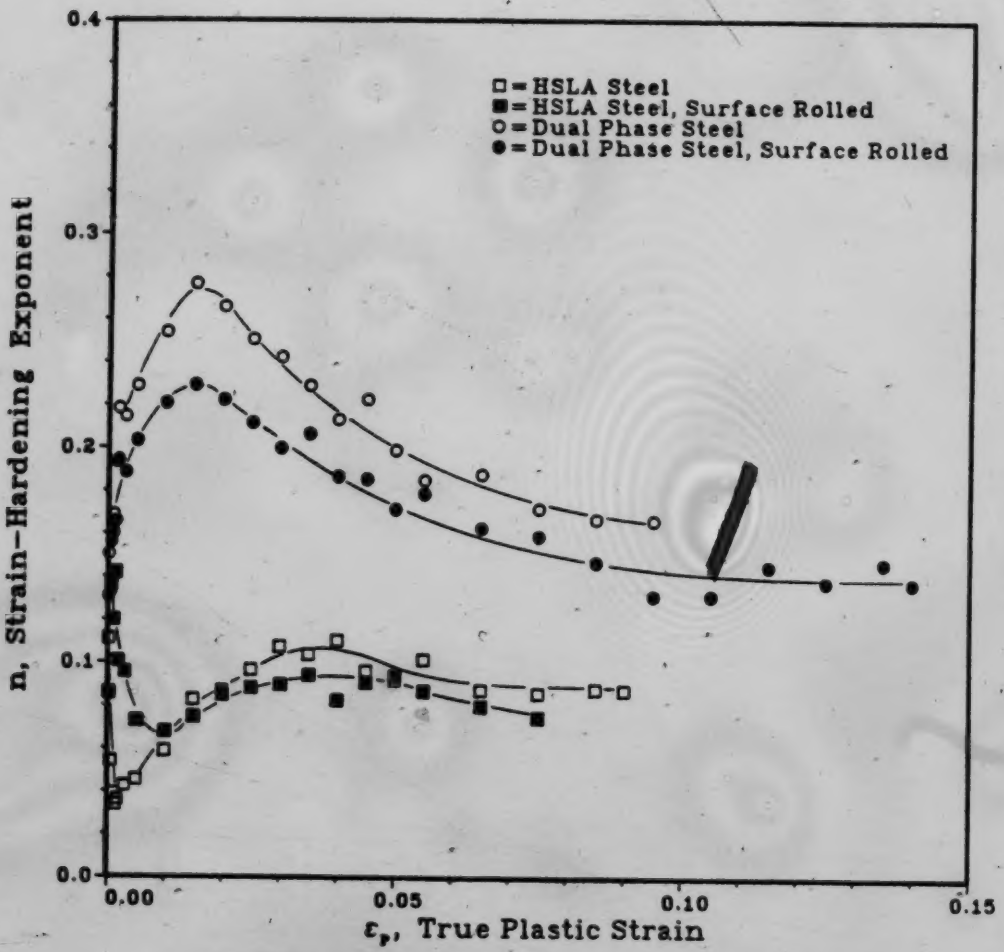

Figure 19: Comparison of the Strain–Hardening Characteristics of the Various Steels.

smaller than 0.01, the HSLA steel's strain hardening exponent is increased slightly (Figure 19) as previously observed in better detail in the logarithmic true stress-true plastic strain curve shown in Figure 17.

5.1.2. Law of Mixtures

Since the dual phase steel is comprised of two major phases, ferrite and martensite, with immmensely different strengths and ductilities, a method of analysis can be applied to consider these two phases as separate components of a composite material. In the dual phase steel, the ferrite yields first with little influence from the martensite. This is followed by plastic deformation of both phases to some varying degree [31, 60]. This behavior is comparable to that of a composite material.

Although the HSLA steel contains different phases, they cannot be considered as separate constituents of a composite material. The HSLA steel deforms in each phase during loading in a bulk manner. Therefore, a composite material analysis cannot be applied to the HSLA steel.

The law of mixtures has been considered in many empirical equations and continuum mechanics models as a method to partition the stress and/or strain between two phases; such as, with the dual phase steel [65]. Using this procedure, it is possible to estimate the "strength" of a composite material. These expressions are:

$$\sigma_C = V_M\sigma_M + (1-V_M)\sigma_F \qquad (8)$$

$$\varepsilon_C = V_M\varepsilon_M + (1-V_M)\varepsilon_F \qquad (9)$$

where σ is the true stress, ε is the true plastic strain and the subscripts C, M, F represent the composite, martensite and ferrite respectively. The law of mixtures predicts a linear relationship between the stress or strain and the volume fraction of the martensite. This is applicable to the dual phase steel [66]. Several variations of equations (8) and (9) occur in the modelling of the deformation behavior of the dual phase steel. These are: isostrain, isostress and an intermediate condition.

5.1.3. Models based on Continuum Mechanics

5.1.3.1. Isostrain Condition

With the assumption of equal strain in both phases, the stress between the two phases can be partitioned as shown in equation (8). Next, the tensile stress-strain curves are approximated by a power function, equation (4). The condition of plastic instability is then applied to obtain the volume fraction as a function of the critical or uniform strain. Thus, the ultimate tensile strength of a two phase composite can be determined from the known tensile behavior of both phases [67, 68].

The model developed by Mileiko [67] has been shown to correlate reasonably well to the experimental flow

characteristics of a dual phase steel [36, 65, 66]. In Figure 20, the composite theory of Mileiko is shown along with the test materials used in this study. The dual phase steel's ultimate tensile strength is in good agreement with the theory. The HSLA steel in either condition was not expected to agree with the theory because it cannot be characterized as a composite material.

5.1.3.2. Strain Partitioning Condition

The previously discussed isostrain models require that there is:

1. elastic and plastic isotropy
2. a perfect continuum at the interfaces
3. no residual stresses
4. the interface does not deform

as stated by Korzekwa et al. [65]. The dual phase steels, in general, do not fulfill the criteria required by the isostrain condition [65]. Thus, eventhough this condition predicts the ultimate tensile strength with some accuracy, it will not describe the total deformation behavior of the dual phase steel.

Therefore, a model based upon an intermediate law of mixtures is required such that the strain is partitioned between the two phases along with the stress [69].

Several strain partitioning models have been developed using different methods of analysis [67-75].

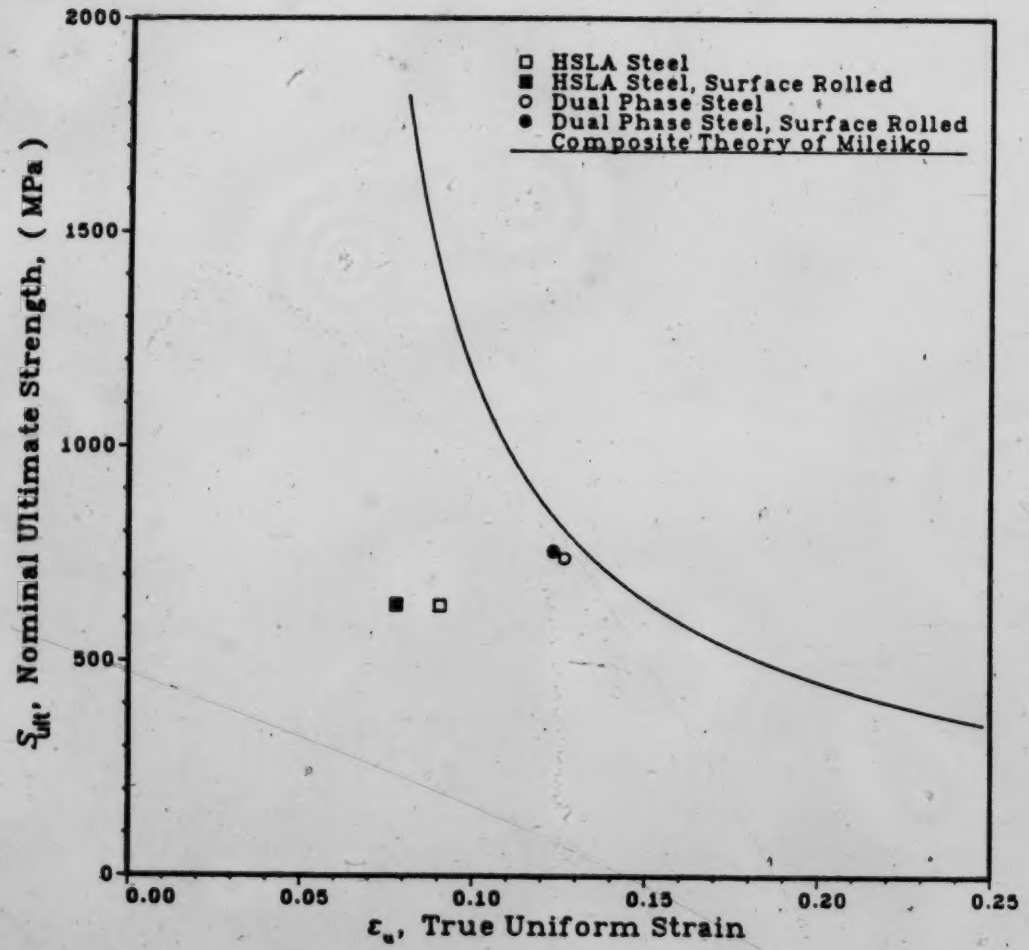

Figure 20: Mileiko's Theory of Composites compared to the Test Materials.

With models based upon continuum mechanics, the strain can be partitioned between the two phases in the composite using several different concepts consisting of: the stored internal energy [70], an inhomogeneous distribution of strain around randomly dispersed particles [71], a parameter defined as the ratio of mean strains of the two phases in the composite [72], a linear partitioning of applied stress [73] or a combination of the previously mentioned [74, 75]. All these models use either linear work hardening or Hollomon's equation to describe the tensile properties of the constituents of the composite.

These theoretical equations in some instances accurately predict the plastic flow of a dual phase steel. When compared to the simple empirical equations, these continuum mechanics models do not provide greater insight into the strain hardening characteristics of a material because they are based on the power curve equation. The complexity of these relationships hinder their application to physical problems. Since they are only applicable to two phase composite materials, the HSLA steel cannot be described by these theoretical equations. Therefore, in order to compare the strain hardening characteristics of both test materials with the same method of analysis, the power curve equation will be used.

5.2. Theoretical Consideration of Indentation

The process of surface rolling is an axisymmetric indentation of a cylindrical shaped material by a smooth rigid toroidal roller. This indentation produces work hardening of the surface layer and a residual stress distribution. In order to understand the mechanisms, the relative magnitudes and the development of residual stress and work hardening by surface rolling, a theoretical analysis of this process is required to aid in the explanation of the experimental results concerning different strain hardening materials in a more analytical and quantitative manner.

5.2.1. The Problem of Indentation

A simplified analysis will be first considered followed by further detailed developments. The surface rolling process can be approximated as an indentation of a body by a rigid sphere. It will also be assumed that the analysis of any blunt indenter is applicable; such as, a flat circular or rectangular punch and the Vickers pyramid.

Also, the material will first be assumed to flow in a rigid-perfectly plastic manner. Further refinements to the theoretical model will be achieved by comparison to experimental observations. These will include the effects of elasticity, compressibility and work hardening.

5.2.1.1. Slip-Line Field Solution

For simplicity, strain hardening is neglected and the elastic strains within the indented body are assumed to be small in comparison to the plastic strains; therefore, the mechanical behavior is modelled as rigid-perfectly plastic as a first approximation. Plasticity theory can then be easily applied in the situation of plane strain and, with further assumptions, axisymmetric conditions can be solved.

A complete solution of the deformation of a rigid-perfectly plastic body by a rigid indenter requires that the stress field be statically admissable and the velocity field be kinematically admissable. A statically admissable stress field is one that satisfies the equations of equilibrium throughout the bodies, the stress boundary conditions and it does not violate the yield criterion. A kinematically admissable velocity field is one that satisfies the incompressibility requirements and the velocity boundary conditions [42, 76-78].

Considering the plane strain stress equations which include the equilibrium equations and the yield criterion, a hyperbolic partial differential equation is obtained which may be solved by the method of characteristics. The stress equilibrium equations corresponding to the characteristics are:

$$P + 2K\varphi = \text{constant on a } \alpha\text{-line} \qquad (10)$$

$$P - 2K\varphi = \text{constant on a } \beta\text{-line} \qquad (11)$$

where α and β are the directions of the two families of characteristics, P is the hydrostatic pressure, K is the pure shear yield stress and φ is the angle turned by the characteristic curve or slip-line. These two relationships are referred to as the Hencky equations [76, 77].

Next, the same procedure may be performed on the velocity equations and one obtains:

$$du - vd\varphi = 0 \text{ on a } \alpha\text{-line} \qquad (12)$$

$$dv + ud\varphi = 0 \text{ on a } \beta\text{-line} \qquad (13)$$

where u and v are the velocity components in the α and β directions respectively. These are known as the Geiringer equations [76, 77].

Hence, by constructing a slip-line field which is both statically and kinematically admissable, the Hencky and Geiringer equations may be solved along the characteristic curves to obtain a distribution and magnitudes of hydrostatic pressure and also, the corresponding velocity field (Figure 21).

This method of analysis becomes more involved for axisymmetric problems. The above stated equations become complicated and the circumferential stress must be assumed to be equal to one of the principal stresses on a meridonal plane during plastic flow (Haar and von Karman hypothesis) [42, 76, 77].

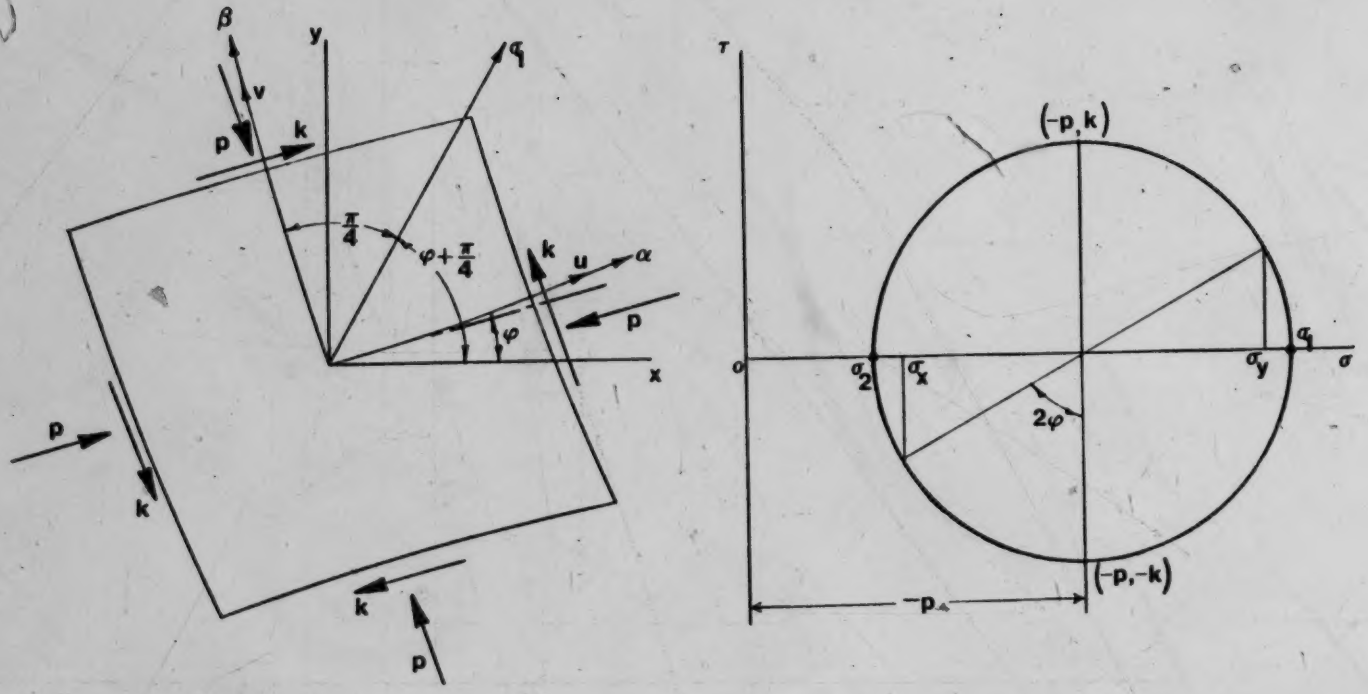

Figure 21 : The Stress System in Plane Plastic Flow [77].

5.2.1.2. Correlation of Theory with Experiment

The slip-line method was first investigated since it provides a relatively easy scheme of obtaining an analytic solution to the problem of indentation of a plastic body by a punch using numerical methods [42, 76, 77, 79]. These methods were also compared using experimental techniques with indenters of different shape [80-82]. From these experiments, it was observed that the plastic flow of materials is not adequately described by the rigid-perfectly plastic model. The initial resulting plastic flow produced by a blunt indenter is much different for a strain hardening material when compared to the flow field predicted by the rigid-perfectly plastic theory as shown in Figures 22 and 23 [83]. Nevertheless, the slip-line solution may be experimentally obtained by placing a thin layer of plasticine on a rigid plate; therefore, the assumptions of the theory must be satisfied to be applicable to the physical situation.

The effects of elasticity and work hardening play an important role in the deformation produced by an indenter. The rigid-perfectly plastic slip-line field predicts quite accurately the distribution of plastic flow around a sharp wedge indentation. But, as the wedge angle is increased to that of a blunt indenter, it is observed that the plastically deformed zone, in the shape of hemispherical surfaces of constant strain, deviates greatly from the

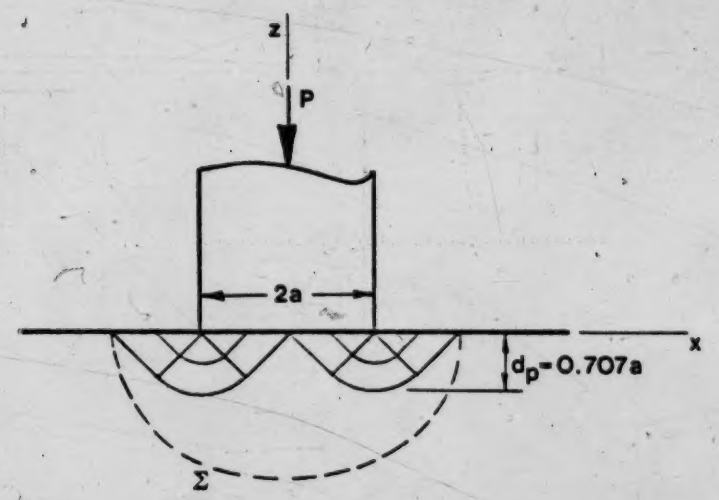

Figure 22 : Plane Strain Slip–Line Field for a Blunt Indenter.

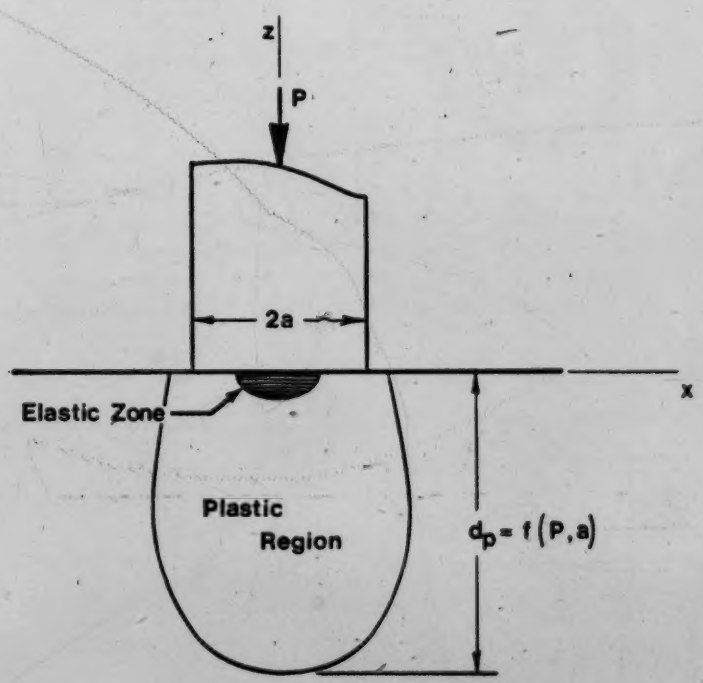

Figure 23 : Plastic Zone for a Strain Hardening Material produced by Blunt Indentation.

basically side flow orientated slip-line solution [84]. This effect becomes greater as the wedge angle approaches that of a blunt indenter.

The rigid-plastic slip-line theoretical treatment is mainly concerned with the boundary between the plastically deformed and rigid materials. In a real material, this boundary does not enclose the total plastic region, since there is a further zone where the plastic and elastic strains are of comparable magnitude. Also, this theory assumes that the displaced material is pushed out to form a "lip"; whereas, the effect of compressibility exists in real materials which decreases this outward flow [85].

This was also observed when the theoretical slip-line field solution for a conical indenter was compared to experimental results [86]. It was stated that friction, elastic strain, work hardening and compressibility must be considered to fully understand their roles and contributions to plastic flow [86].

Since the slip-line field theory cannot predict the existence of residual stress, elastic effects must be considered to improve the theoretical model. Basically, in this model, the Hertz constant shear lines were matched with the concentrated load shear lines from the Boussinesq solution to obtain an approximate solution to the problem. This method was chosen because the experimental plastic boundary strongly resembles a line of constant maximum shear stress beneath a frictionless blunt punch [85]. This

distribution was also determined experimentally with microhardness tests across the plastic zone [83]. The improved solution provides a constraint factor of P/Y = 3 for an elastic-perfectly plastic material subject to axisymmetric blunt indentation [87, 88]. The major drawback with this new method is that the process of blunt indentation is assumed to be unaltered by the effects of strain hardening. Also, the plastic flow which occurs has no effect upon the applied load, the stresses and the position of the elastic-plastic boundary.

Thus, a detailed theory for the deformation beyond the yield point, which considers elastic behavior and strain hardening, is still lacking. Since the behavior of plastic flow is dependent on the path of loading, it becomes necessary to follow the deformation with time when modelling real materials.

The finite element method of analysis provides a formulation to study the elastic-plastic behavior of axisymmetric problems. This method can take into account realistic friction conditions and actual material properties. It also reveals the development and boundary of the plastic zone along with the magnitudes and distributions of stress and strain. Upon un-loading, the residual stresses can be determined. Therefore, the finite element method will create a better overall picture of axisymmetric indentation of a real material than the previously discussed models.

The above procedure has been applied to several axisymmetric indentation problems [89-92]. These solutions correlate quite well with experimental results. The shape of the plastic zone is basically a hemispherical surface which was observed to occur using experimental methods; such as, grids or etching [84, 87, 88]. Thus, the finite element method provides an "accurate" procedure for analyzing the problem of indentation even though the material may only be treated as elastic-perfectly plastic or elastic-linear work hardening.

Another method available for analyzing the indentation of a strain hardening material is to use an experimentally determined shear strain distribution to aid in the development of a slip-line field solution. The stress equilibrium equations (equations (10) and (11)) may be extended to include strain hardening terms as shown:

$$\Delta P = -2K\Delta\varphi + \frac{\Delta K}{\Delta s_2}\Delta s_1 \quad \text{along a } \alpha\text{-line} \qquad (14)$$

$$\Delta P = +2K\Delta\varphi + \frac{\Delta K}{\Delta s_1}\Delta s_2 \quad \text{along a } \beta\text{-line} \qquad (15)$$

where s_1 and s_2 are the distances along slip-lines. Using the Hollomon equation to describe the yield strength, the distribution of hydrostatic pressure, P can be calculated from the known shear strain distribution [93].

Both the above and the finite element method are too complex to apply easily to the surface rolling procedure used in this study. Consequently, it was decided to use various ideas and concepts from the previously discussed

methods of analysis along with limit theory to explain the effect of strain hardening on the depth of penetration of cold work due to surface rolling.

5.2.2. Applying the Indentation Theory to the Results

In summary, the depth of penetration of cold working produced by surface rolling is dependent on the strain hardening characteristics of the material [80-88]. For the model materials used in this study, the effect of plastic flow behavior on the penetration depth was observed experimentally by using microhardness measurements as shown in Figure 10. This relationship between strain hardening and surface rolling penetration depth can be explained to some degree using theoretical results.

In applying a theoretical analysis, the mathematical modelling of work hardening presents several complexities in attempting to explain the true material behavior. In most mathematical treatments, the strain hardening characteristics are generalized to either a perfectly plastic or a linear work hardening model. This analysis is not accurate in this situation since the dual phase steel strain hardens from the onset of loading as shown in Figures 8 and 17.

These simplified models can be applied to the HSLA steel as a crude approximation. Recall that the HSLA steel has a low rate of strain hardening as shown in Figures 17 and 19. Thus, an elastic-perfectly plastic material

behavior may be assumed to model the HSLA steel since the logarithmic stress-strain curve is almost horizontal in comparison to that of the dual phase steel (Figure 17).

Therefore, the "theoretical" analysis will be concentrated on explaining the indentation of HSLA steel. Using the assumed plastic flow behavior, limit theory can be applied to the HSLA steel along with a qualitative analysis to understand and explain the plastic flow depth of an indentation process. These results can then be extrapolated to describe the surface rolling of dual phase steel.

5.2.2.1. Limit Theory

An approximate method denoted as limit theory is used to estimate an upper and lower bound. This is due to the lack of exact solutions which can determine the load to produce unconstrained plastic deformation for the model materials used in this study of surface rolling.

An upper bound is obtained by establishing a kinematically admissable velocity field with the equilibrium of stresses unsatisfied in some regions. A lower bound is found by developing a statically admissable stress field with the velocity conditions not satisfied in the material [76-78, 94].

Applying these two theorems to the indentation of a body by an axisymmetric blunt punch, the load range is determined to be $5.00 \geq P/K \geq 5.71$ where P is the applied

pressure and K is the Tresca shear yield stress [78, 94]. The simplified slip-line field used by the limit theories is shown in Figures 24 and 25.

An approximate quasi-upper bound was calculated for a rigid spherical indenter by equating the Hertz and Boussinesq solutions in an empirical manner to obtain a constraint factor of P/Y = 3 [88]. Using the Tresca yield condition, this is equal to P/K = 6.

Using this pressure corresponding to 6K for a spherical indenter for the surface rolling process, a plastic flow load can be calculated to compare with the actual applied load. From the Hertz theory of contact stress [95], the maximum pressure is:

$$P = \frac{3F}{2\pi a^2} \qquad (16)$$

where F is the applied load and a is the contact radius. Assuming a circular indentation from the toroidal shaped surface roller, the radius, a can be determined , if the elastic springback of the deformed zone is neglected, from the scans of surface roughness shown in Figure 9. The calculated load to produce plastic flow is 143 N for the HSLA steel; whereas, the experimental load was 178 N.

When plastic flow begins for the rigid-plastic case, the penetration depth is basically constant with most of the plastic deformed material being displaced to the sides of the indenter. As the amount of strain hardening is increased from the perfectly-plastic behavior, the

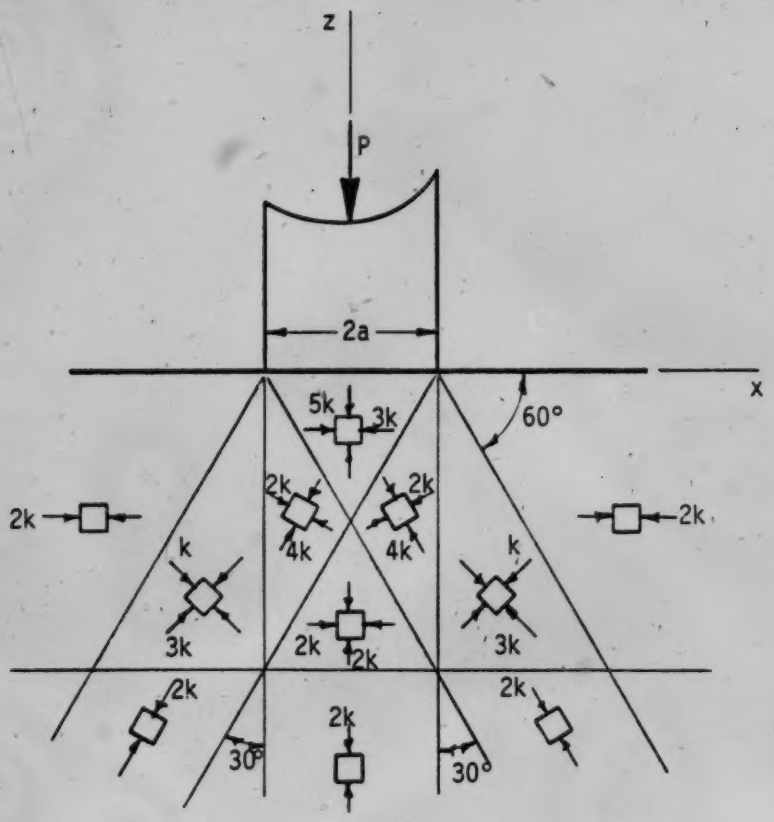

Figure 24 : A Limit Theory Statically Admissable Stress Field for a Plane Strain Blunt Indenter.

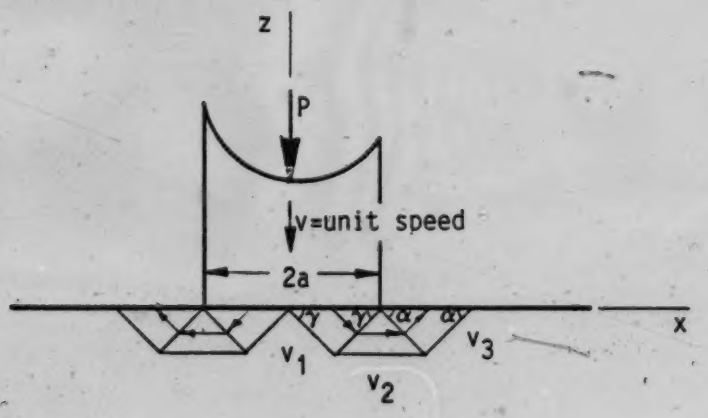

Figure 25 : A Limit Theory Velocity Field for a Plane Strain Blunt Indenter.

penetration depth becomes a strong function of the applied load and the compressibility of the material.

Since the Tresca shear yield stress for the dual phase steel is initially lower than the value for the HSLA steel, the required load to start plastic flow would be smaller. Relatively, the experimental applied load is larger for the dual phase steel in comparison to the HSLA steel.

Since the difference between the required plastic flow load and the load used experimentally is larger for the dual phase steel, the depth of plastic deformation would be greater when compared to the HSLA steel.

Also, the HSLA steel can be more closely modelled as a rigid-plastic material where the deformed zone increases perpendicularily to the applied indenter load. Thus, the plastic zone of the HSLA steel would be smaller when compared to a material with an increased work hardening behavior where the material is compressed in the direction of the applied load.

Hence, an increase in the amount of strain hardening should increase the plastic deformed zone.

5.2.2.2. Effect of Strain Hardening on the Results

The strain hardening characteristics of the two model materials were discussed in section 5.1. It was observed that the dual phase steel had a mean strain hardening exponent which was twice as large as the value for the HSLA

steel. From section 5.3.1., the plastic deformed zone should be influenced by the applied load to a greater extent as the amount of strain hardening is increased.

Thus, the plastic zone for the dual phase steel should be greater than that of the HSLA steel by some function of the difference in their strain hardening abilities. From Figure 10, the measured depth of penetration by surface rolling was 0.57 mm for the dual phase steel compared to 0.33 mm for the HSLA steel. This difference is about 73%.

This is comparable to the 100% difference in the mean strain hardening exponent. Therefore, the increase in the strain hardening exponent approximately reflects the amount of increase to be achieved in the penetration of plastic flow by indentation or, in this situation, surface rolling.

5.2.2.3. Hertz Theory

The Hertz contact stresses can be determined in an approximate manner if the material behavior is assumed to be elastic and the two bodies are spherically shaped. To approximate the rate of work hardening of the model materials, a modulus of elasticity can be defined using the criterion of equal flow stress between the two materials. In one case, the two elastic moduli are equal as with the roller and the HSLA steel. The second case uses a tangent elastic modulus for the dual phase steel which is defined as the slope of the line connecting zero stress to the stress

at 2% elongation where the flow stress is equal to that of the HSLA steel (Figure 8). This tangent modulus is about 10 times less than the elastic modulus of the HSLA steel.

The distribution and magnitude of the shear stress calculated by using the Hertz theory of contact stress will be compared for the two situations. The shear stress is defined as [95]:

$$\tau_{xy} = \frac{4a}{\pi}\left\{ (1+\mu)\left[\frac{z}{a}\cot^{-1}\frac{z}{a} - 1 \right] + \frac{3}{2}\frac{a^2}{a^2+z^2} \right\} \qquad (17)$$

where a is the contact radius,

$$a^3 = \frac{3\,F}{8\,A} \qquad (18)$$

and A is defined as a material parameter;

$$A = \frac{(1/d_1) + (1/d_2)}{[\,(1-\mu_1)/E_1 + (1-\mu_2)/E_2\,]} \qquad (19)$$

The maximum shear stress for each case can be calculated using a roller diameter of 25.4 mm (1 in.) and a specimen diameter of 6.35 mm (0.25 in.) to approximate the actual geometry.

Upon comparison, the maximum shear stress for the approximated dual phase steel case occurs at a depth 60% greater than that for the supposed HSLA steel situation.

From section 5.2., it was stated that the initiation of plastic flow occurred below the surface. Relating this to the depth of the maximum shear stress, the dual phase steel

will develop a greater penetration of plastic deformation since the location of the maximum shear stress is shifted further from the surface than the HSLA steel. Thus, upon expansion of the deformed zone, the dual phase steel will have a much deeper nucleus of plastic flow.

The depth of penetration measured by microhardness was 73% greater for the dual phase steel. This compares favorably to the 60% increase in depth of the location of maximum shear stress calculated by assuming that the Hertz theory of contact stress is applicable to the initial instantaneous loading of the surface rolling mechanism.

5.2.3. Summary of the Indentation Problem

Several arguments were presented in the previous sections using information from the literature [78-86] and comparisons to the experimental results. The predictions obtained from limit theory, the difference in strain hardening exponent and the location of the maximum shear stress all conclude that a higher rate of strain hardening will produce an increase in the penetration of plastic deformation for the same applied load.

5.3. Effect of Plastic Zone Depth on Residual Stress

Since the method of evaluation of the effect of strain hardening on surface rolling is direct stress cyclic

loading, the accumulation of plastic microstrain which can decrease the magnitude of the favorable compressive residual stress with each repeated load cycle is important in determining the amount of improvement to be gained by the fatigue strength of a component by surface rolling [8, 14]. The rate of relaxation of these residual stresses is dependent on the applied load and the strain hardening properties of the material [96, 97].

Basically, the magnitude and the distribution of residual stresses are altered when localized yielding occurs at some region where the sum of the residual and applied stresses exceeds the flow stress of the material [96].

In order to mathematically study the decay of surface residual stress, the relaxation behavior may be approximated as the decay of mean stress due to a constant applied strain. This simplification assumes that the surface layer experiences repeated strain when the component is axially stressed.

With each load cycle, there is a decrease in mean stress because of some accumulated plastic strain as shown by [97];

$$-\frac{1}{E}\frac{d\sigma_N}{dN} = f_p(\sigma_{max}) - f_p(|\sigma_{min}|) \qquad (20)$$

where the plastic strain is defined as a function of the applied stress,

$$\epsilon_p = f_p(\sigma) , \qquad (21)$$

E is the modulus of elasticity, N is the number of cycles and σ_N is the residual stress at N cycles. This result can be integrated to obtain a general equation of the form:

$$N = \frac{-1}{E} \int_{\sigma_o}^{\sigma_N} \frac{d\sigma_N}{f_p(\sigma_{max}) - f_p(|\sigma_{min}|)} \qquad (22)$$

With a suitable choice of an equation to define the stress-strain curve, a stress relaxation relationship is obtained by numerical integration of equation (22).

Since this result is too complex to apply easily, an approximate equation was derived from simplifications applied to equation (22) by Morrow et al [96, 97];

$$\frac{\sigma_N}{\sigma_o} = \frac{\sigma_1}{\sigma_o} - \left(\frac{\sigma_a}{\sigma_y} \right)^b \cdot \log N \qquad (23)$$

where σ_o is the initial residual stress, σ_1 is the residual stress after one load cycle, σ_a is the applied alternating stress and σ_y is the yield strength of the material. This empirical equation was used to describe the longitudinal compressive residual stress relaxation of the HSLA and dual phase steels shown in Figures 14 and 15 respectively.

Linear regression was utilized to determine the constant, b along with the first cycle ratio, σ_1/σ_o which appears in equation (23). The respective empirical equations are:

$$\frac{\sigma_N}{\sigma_o} = 0.66 - \left(\frac{\sigma_a}{\sigma_y} \right)^{6.1} \cdot \log N \qquad (24)$$

for the HSLA steel and,

$$\frac{\sigma_N}{\sigma_o} = 1.20 - \left(\frac{\sigma_a}{\sigma_y} \right)^{8.9} \cdot \log N \qquad (25)$$

for the dual phase steel. These are shown in Figures 26 and 27 along with the respective experimental results.

The first cycle stress ratio, σ_1/σ_o in the empirical equation for the dual phase steel is greater than one. Since the empirical equation was determined using a least squares linear regression, it cannot account for the stability of the compressive longitudinal residual stress during the first 10^2 cycles. The decay of the longitudinal residual stress within the surface layer of the dual phase steel does not begin until approximately 10^2 cycles. Thus, the empirical equation describes the relaxation behavior of the surface rolled dual phase steel for load cycles greater than 10^2.

In comparing the two model materials, the relaxation of the surface residual stress during the first few cycles occurs very quickly in the surface rolled HSLA steel. This is reflected by the first cycle stress ratio which is smaller for the HSLA steel than the value for the dual phase steel.

The stability during the first 10^2 cycles in the surface rolled dual phase steel's longitudinal residual stress can be attributed to a larger depth of penetration of plastic deformation which counteracts the effect of plastic strain accumulation [25, 96].

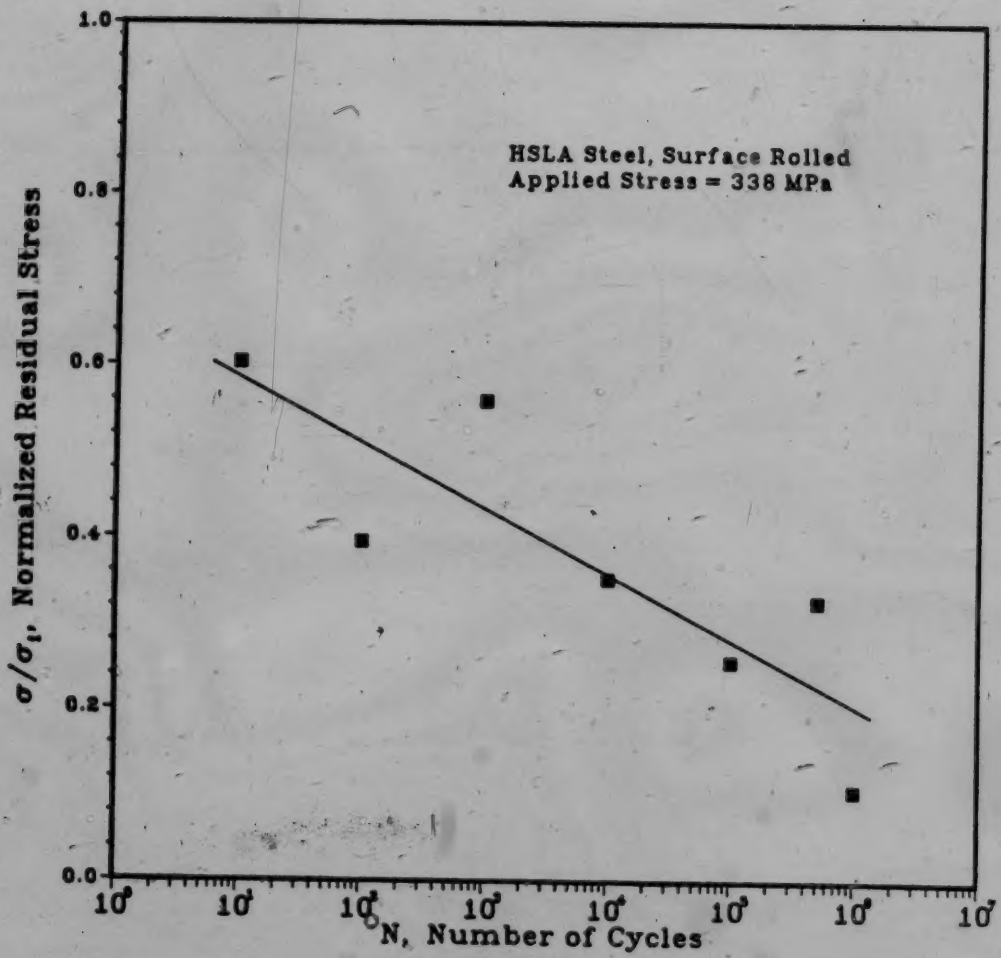

Figure 26: Comparison of Experimental Data of the Relaxation of the Longitudinal Surface Residual Stress with an Empirical Equation for the HSLA Steel.

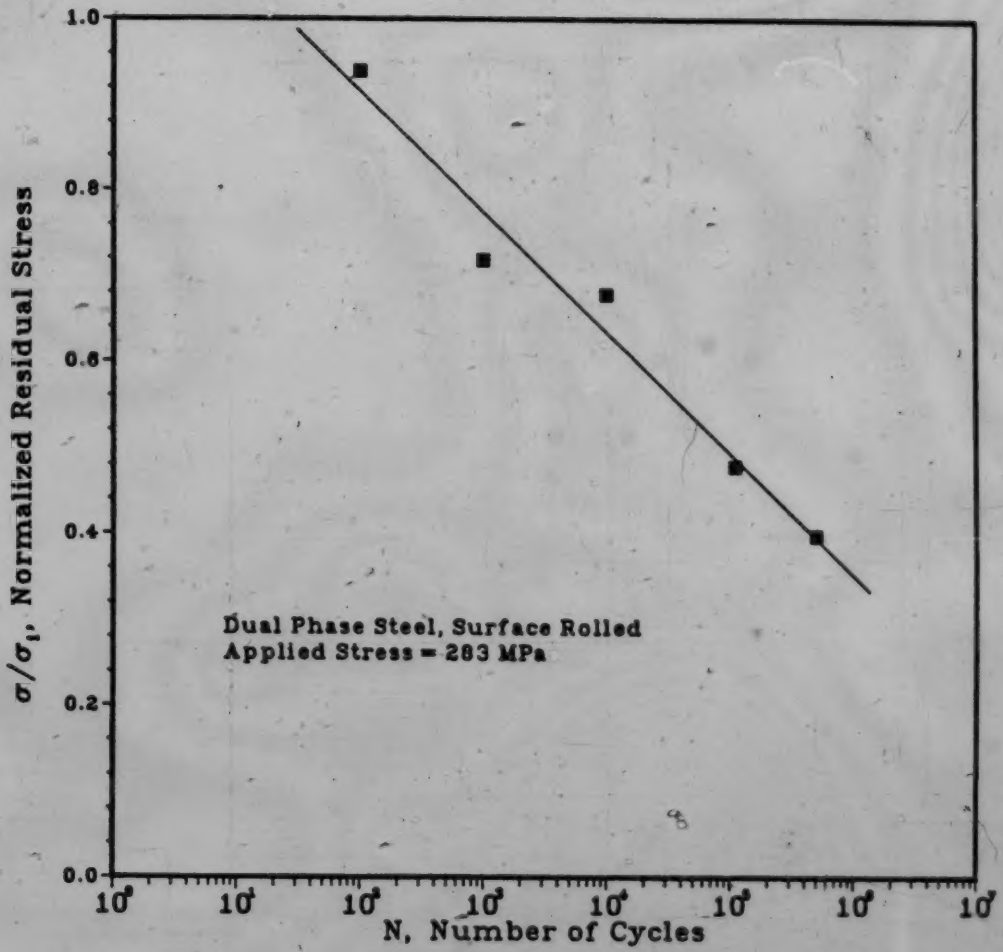

Figure 27: Comparison of Experimental Data of the Relaxation of the Longitudinal Surface Residual Stress with an Empirical Equation for the Dual Phase Steel.

After 10^2 cycles, the rate of relaxation is determined by the constant, b. This constant is larger for the dual phase steel than that of the HSLA steel (8.9 and 6.1 respectively). Therefore, the longitudinal surface residual stress in the dual phase steel relaxes at a rate 1.5 times faster than in the HSLA steel after 10^2 cycles.

The faster decay after 10^2 cycles for the dual phase steel is explained by examining the plastic strain defined by equation (22). For the dual phase steel, plastic strain occurs at a much lower flow stress in comparison to the HSLA steel. The higher rate of strain hardening and the low initial yield strength of the dual phase steel will increase the amount of accumulated plastic strain which relaxes the residual stress.

Thus, there must be enough plastic strain accumulated during cyclic loading to decrease the effective size of the work hardened zone in order for the compressive residual stress to begin relaxing.

Hence, the deeper penetration of plastic flow in the surface rolled dual phase steel provides a larger strengthened surface layer and a greater surface volume affected by residual stress. This promotes the stability of the compressive residual stresses in the surface layer during a cyclically varying applied axial load [25, 96].

5.4. Strain Hardening, Surface Rolling and Fatigue

The effect of strain hardening on surface rolling was shown to be quite considerable in section 5.2.2. An increase in the strain hardening characteristics of a material provided an increase in the extent of the plastic deformed zone produced by surface rolling as shown in Figure 10.

Also, the longitudinal compressive residual stress created by the surface rolling procedure were larger in the dual phase steel when compared to the HSLA steel as shown in Table 2 (670 MPa and 629 MPa respectively). These residual stresses in the dual phase steel did not relax as quickly as the residual stresses within the HSLA steel during the first thousand loading cycles. After 10^2 cycles, the dual phase steel's longitudinal compressive residual stress decayed at a faster rate. Although at all times, it was greater in magnitude as shown in Figures 26 and 27.

With the larger work hardened zone and the larger compressive residual stresses contained in the dual phase steel, it still did not lead to a stronger effect of surface rolling on improving the direct stress fatigue strength of the dual phase steel when compared to the HSLA steel as shown in Figure 16. There was only a 7% increase in the fatigue strength at 10^7 cycles for the surface rolled dual phase steel compared to a 13% increase for the surface rolled HSLA steel.

This may be explained by a shift in the location of crack initiation in the surface rolled dual phase steel specimens. In Figure 28, the fracture surfaces of two different specimens for both the surface rolled dual phase and HSLA steels are shown. It was observed with several test specimens that the dual phase steel's fracture surface has a "lip" along the edge with a sub-surface fracture origin located slightly inwards from the "lip". This is approximately the interface of the plastically deformed zone and the core material [7, 28, 29].

A sub-surface fatigue crack initiation at this interface will also occur with the HSLA steel but the distance from the surface is smaller due to the lower depth of penetration of plastic deformation by surface rolling.

Further strengthening of the dual phase steel by surface rolling may increase the direct stress fatigue strength of the surface layer but it will not significantly alter that of the core material. Therefore, this indicates that there exists an upper bound to the amount of improvement to be gained from surface rolling the dual phase steel. Once the "strength" of the surface grains have been increased to the level of the bulk material, the direct stress fatigue strength of this bulk material will begin to control the life of the component when subjected to a cyclically varying direct stress.

Applied pressures greater than the 178 N load used in this study will create a larger work hardened zone, but upon

a). HSLA Steel, Surface Rolled

b). Dual Phase Steel, Surface Rolled

Figure 28 :Comparison of the Fatigue Failure Fracture Surfaces of the Surface Rolled Dual Phase and HSLA Steels.

cyclic loading, the crack will initiate at the approximate interface of the plastically deformed zone and the base material. At this interface, the residual stress becomes tensile within the core [29]. With a larger plastic zone, the tensile residual stress of the core must increase to satisfy equilibrium. This increase in the core residual stress will cause the yield strength of the core to be exceeded earlier during cyclic loading [7, 28, 29]. Thus, the relationship between the yield strength of the core and the residual stress induced within the core material will start to control the fatigue improvement by surface rolling [29].

Hence, further improvement beyond the amount obtained in this study of the direct stress fatigue strength of the dual phase steel is not possible with surface rolling because the crack will initiate inside of the specimen instead of the surface. Therefore, the bulk properties of the core material become important again in determining the fatigue life of the component.

Although for bending or torsion fatigue, there may be greater improvement from surface rolling, since the applied stress is not constant across the cross-section but it varies linearly from zero at the center to some value at the surface. Thus, the core material is subjected to a much smaller applied load than the surface layer. Therefore, an increase in the depth of penetration of surface rolling will enable the component to withstand a greater load since the

core is stressed to a reduced load dependent on the geometry and material properties of the metal part. If a load corresponding to the core material fatigue strength could be applied to the core, the surface layer would observe a higher stress due to the linear relationship of stress for both bending and torsion. Consequently, the improvement in fatigue life of a metal component by surface rolling will be greater for bending or torsion fatigue in comparison to direct stress fatigue.

6. Conclusions

The results obtained through this study of the influence of strain hardening characteristics on the depth of penetration of surface rolling and the effectiveness of the mechanical surface treatment on improving the direct stress fatigue strength allow the following conclusions to be drawn:

(1.) There is a correlation between the strain hardening characteristics and the depth of the plastic zone produced by surface rolling.

(2.) The strain hardening behavior of the dual phase and HSLA steels cannot be represented by a single power function.

(3.) Strain hardening does not improve the direct stress high cycle fatigue strength of the dual phase steel to the level of the HSLA steel.

(4.) The potential strain hardening of the dual phase steel does not lead to a stronger effect of surface rolling on increasing the direct stress fatigue strength. This is due to a shift in the location of crack initiation from the surface to the interface of the work hardened zone and the base material.

References

[1] ASM Committee on Shot Peening, "Shot Peening and Other Surface Working Processes", Metal Progress, July 15, 1954, pp. 104-108.

[2] Cable, C.W., "Theory of Surface Rolling for Fatigue Improvement", Surface Rolling and Other Methods for Mechanical Prestressing of Metals - SAE J811, chapter 2, 1962, pp. 6-10.

[3] Neifert, H.R., "Calculations for the Surface Rolling Process", Surface Rolling and Other Methods for Mechanical Prestressing of Metals - SAE J811, chapter 3, 1962, pp. 11-19.

[4] von Finckenstein, E. and Preckel, U., "Internal Stresses produced by Fine Surface Rolling", Stahl u. Eisen, v. 104, n. 14, July 1984, pp.657-660.

[5] Burrell, N.K., "Calling the Shots that Kill Fatigue", American Machinist, April 1981, pp. 119-122.

[6] Niku-Lari, A., "Shot-Peening", First International Conference on Shot Peening, ed. A. Niku-Lari, Pergamon Press, 1982, pp. 1-21.

[7] Hu Nai-Sai and Zhou Hui-Jiu, "The Effect of Surface Plastic Deformation on Fatigue Strength and Its Mechanism", First International Conference on Shot Peening, ed. A. Niku-Lari, Pergamon Press, 1982, pp. 351-357.

[8] Koibuchi, K., Hayama, T. and Kawai, S., "Residual Stress and Fatigue Strength of Surface Hardened Components", First International Conference on Shot Peening, ed. A. Niku-Lari, Pergamon Press, 1982, pp. 413-419.

[9] Al-Hassini, S.T.S., "Mechanical Aspects of Residual Stress Development in Shot Peening", First International Conference on Shot Peening, ed. A. Niku-Lari, Pergamon Press, 1982, pp. 583-602.

[10] Wohlfahrt, H., "Shot Peening and Residual Stress", Residual Stress and Stress Relaxation, ed. E. Kula and V. Weiss, New York : Plenum Press, 1982, pp. 71-92.

[11] Al-Hassini, S.T.S., "The Shot Peening of Metals - Mechanics and Structures", Shot Peening for Advanced Aerospace Design - SP-528, Society of

Automotive Engineers, Inc., 1982, pp. 1-13.

[12] Niku-Lari, A., "Residual Stresses and Surface Finish in Shot-Peened Components and Materials", Experimental Techniques, February 1983, pp. 30-36.

[13] Niku-Lari, A., "Influence of Residual Stresses Introduced by Shot-Peening Upon Fatigue Life of Materials", Experimental Techniques, March 1983, pp. 21-25.

[14] Dolan, T.J., "Residual Stress, Strain Hardening and Fatigue", Internal Stresses and Fatigue in Metals, ed. G.M. Rassweiler and W.L. Grabe, Elsevier Publishing Co., 1959, pp. 284-310.

[15] James, M.R. and Morris, W.L., "Fatigue Induced Changes in Surface Residual Stress", Scripta Metallurgica, v. 17, 1983, pp. 1101-1104.

[16] Frost, N.E., Marsh, K.J. and Pook, L.P., "Metal Fatigue", Oxford University Press, 1974.

[17] MacGregor, C.W., "The Significance of Residual Stresses", Residual Stresses in Metals and Metal Construction, ed. W.R. Osgood, New York : Reinhold Publishing Corp., 1954, pp. 103-126.

[18] Horger, O.J. and Neifert, H.R., "Correlation of Residual Stress with Fatigue Strength of Machine Elements and Related Phenomena", Residual Stresses in Metals and Metal Construction", ed. W.R. Osgood, New York : Reinhold Publishing Corp., 1954, pp. 219-253.

[19] Hempl, M.R., "Surface Condition and Fatigue in Metals", ed. G.M. Rassweiler and W.L. Grabe, Elsevier Publishing Co., 1959, pp. 311-334.

[20] Baldwin Jr., W.M., "Residual Stresses in Metals", Edgar Marburg Lecture, ASTM, v.49, 1949, pp. 1-45.

[21] ASM Committee on Residual Stress, "Residual Stresses", Metal Progress, August 15, 1955, pp. 89-96.

[22] Almen, J.O. and Black, P.H., "Residual Stress and Fatigue in Metals", New York : McGraw-Hill Book Company, 1963.

[23] Dieter, G.E., "Mechanical Metallurgy", Toronto : McGraw-Hill, Inc., Second Edition, 1976.

[24] Mattson, R.L. and Roberts, J.G., "The Effect of

Residual Stresses Induced by Strain Peening upon Fatigue Strength", Internal Stresses and Fatigue in Metals, ed. G.M. Rassweiler and W.L. Grabe, Elsevier Publishing Co., 1959, pp. 337-360.

[25] James, M.R., "The Relaxation of Residual Stress During Fatigue", Residual Stress and Stress Relaxation, Sagmore Army Materials Research Conf. Proc., ed. E. Kula and V. Weiss, New York : Plenum Press, 1982, pp. 297-314.

[26] Van Vlack, L.H., "Elements of Materials Science and Engineering", Addison-Wesley Publishing Co., Fourth Edition, 1980.

[27] Parker, E.R., "Strain Hardening", The Strengthening of Metals, ed. D. Peckner, New York : Elsevier Publishing Corp., 1964.

[28] Kettunen, P.O. and Kocks, U.F., "Fatigue Hardening and Fatigue Life", Acta Metallurgica, v. 20, Jan. 1972, pp. 95-103.

[29] Luther, R.G. and Williams, T.R.G., "Influence of Surface Reinforcement on the Fatigue Strength of Low Carbon Steel", Metallurgia and Metal Forming, March 1974, pp. 72-77.

[30] ASTM, "Standard Methods for determining Average Grain Size", ASTM Standard E112-84, pp. 117-149.

[31] Rashid, M.S., "Dual Phase Steels", Annual Reviews of Material Science, v. 11, 1981, pp. 245-266.

[32] Speich, G.R., "Physical Metallurgy of Dual-Phase Steels", [Proc. Conf.] The Heat Treatment Committee of The Metallurgical Society of AIME and the ASM/MSD Structures Activity Committee, 1981, pp. 3-45.

[33] Magee, C.L. and Davies, R.G., "Automotive Sheet Steels for the 1980's", Alloys for the Eighties, Climax Molybdenum Company, Chairman: H.N. Lander, Editor: R.Q. Barr, pp. 25-34.

[34] Drewes, E.J., "Experience with the Production and Application of As-Rolled Dual Phase Steel", Alloys for the 1980's, Climax Molybdenum Company, Chairman: H.N. Lander, Editor: R.Q. Barr, pp. 59-67.

[35] Rashid, M.S., "GM980X - Potential Applications and Review", SAE Transactions, 1977, pp. 935-946.

[36] Davies, R.G., "Influence of Martensite Composition and Content on the Properties of Dual Phase Steels", Metallurgical Transactions, v. 9A, May 1978, pp. 671-679.

[37] Jacquet, P.A., "Electrolytic and Chemical Polishing", Metallurgical Reviews, v. 1, part 2, 1956, pp. 157-238.

[38] Liu, C.R. and Barash, M.M., "Variables Governing Patterns of Residual Stress in a Machined Surface", Trans. ASME, Journal of Engineering for Industry, v. 104, August 1982, pp. 257-264.

[39] Koster, W.P., "Observations on Surface Residual Stresses vs. Fatigue Strength", Metcut Research Associates, Inc., Bulletin 677-1, 1977.

[40] Freudenthal, A.M., "The Inelastic Behavior of Engineering Materials and Structures", New York : John Wiley & Sons, Inc., 1950.

[41] Timoshenko, S., "Strength of Materials, Part II : Advanced Theory and Problems", Princeton, N.J. : D. van Nostrand Co. Ltd., Third Edition, 1956, pp. 346-381.

[42] Prager, W. and Hodge, P.G., "Theory of Perfectly Plastic Solids", New York : John Wiley & Sons, Inc., 1951.

[43] Forrest, G., "Residual Stresses in Beams after Bending", Symposium on Internal Stresses in Metals and Alloys, Institute of Metals, 1947, pp. 153-162.

[44] Siemens, "Preparation Technique for X-Ray Spectrometry", Reprint from Zerstorungsfreie Materialprufung (section U 152), Eg4/202e, July 1967, 15p.

[45] Siemens, "Flat Camera for Stress Measurements", Bereich Meβ- und Prozeβtechnik, Karlsruhe, Eg4 A303/1e, July 1972, 11p.

[46] Thomas, D.E., "Measurement of Internal Stresses by X-Rays", Symposium on Internal Stresses in Metals and Alloys, Institute of Metals, 1947, pp. 25-30.

[47] Ernst Leitz GMBH Wetzlar, "A Guide for Working with the Miniload-Hardness Testor".

[48] ASTM, "Standard Test Method for Microhardness of Materials", ASTM Standard E384-73, pp. 373-393.

[49] Mott, B.W., "Micro-Indentation Hardness Testing", London : Butterworths Scientific Publications, 1956.

[50] ASTM, "Standard Methods of Preparation of Metallographic Specimens", ASTM Standard E3-80, pp. 15-21.

[51] Bowden, F.P. and Moore, A.J.W., "Internal Stresses produced by the Sliding of Metals", Symposium on Internal Stresses in Metals and Alloys, Institute of Metals, 1947, pp. 131-137.

[52] ASM Committee on Metallography of Wrought Stainless Steels, "Metals Handbook", ASM, 8th Edition, v. 8, 1961, p. 98.

[53] Krupitzer, R.P., "Strain Aging Behavior in a Continuously-Annealed, Dual-Phase Steel", Fundamentals of Dual-Phase Steels, The Metallurgical Society of AIME, ed. R.A. Kot and B.L. Bramfitt, 1981, pp. 315-330.

[54] Barrett, C.S., "Structure of Metals : Crystallographic Methods, Principles and Data", New York : McGraw-Hill Book Co., Inc., Second Edition, 1952.

[55] Cullity, B.D., "Elements of X-Ray Diffraction", Reading, Mass.: Addison-Wesley Publishing Company, Inc., 1959.

[56] Taylor, A., "X-Ray Metallography", New York : John Wiley & Sons, Inc., 1961.

[57] Lonsdale, D., Doig, P. and Flewitt, P.E.J., "X-Ray System for Stress Measurements", Engineering Digest, v. 31, n. 7, August 1985, pp. 32-34.

[58] Thomas, D.H. and Bell, T., "Fatigue Behavior of Aged Gas-Nitrocarburized Low-Carbon Steel", Metal Science, v. 14, February 1980, pp. 73-78.

[59] Hollomon, J.H., "Tensile Deformation", AIME Trans. of the Iron and Steel Division, v. 162, 1945, pp. 268-290.

[60] Tomita, Y. and Okabayashi, K., "Tensile Stress-Strain Analysis of Cold Worked Metals and Steels and Dual-Phase Steels", Metallurgical Transactions A, v. 16A, May 1985, pp. 865-872.

[61] Mullins, S., "Deformation Behavior of Titanium Sheet Metal", B.Sc. Thesis, Kreble College,

Oxford, 1978.

[62] Monteiro, S.N. and Reed-Hill, R.E., "On the Double-n Behavior of Iron", Metallurgical Transactions, v. 2, October 1971, pp. 2947-2948.

[63] Huang, M. Luo, J. and He, B., "Some Problems about Strain Hardening Exponent of Metals", Mechanical Behavior of Metals - IV, ed. J. Carlsson and N.G. Ohlson, Pergamon Press, v. 2, 1984, pp. 673-680.

[64] Matlock, D.K., Krauss, G., Ramos, L.F. and Huppi, G.S., "A Correlation of Processing Variables with Deformation Behavior of Dual-Phase Steels", Structure and Properties of Dual-Phase Steels, ed. R.A. Kot and J.W. Morris, Proc. Conf. of AIME, New Orleans, 1979, pp. 62-90.

[65] Korzekwa, D.A., Lawson, R.D., Matlock, D.K. and Krauss, G., "A Consideration of Models describing the Strength and Ductility of Dual-Phase Steels", Scripta Metallurgica, v. 14, 1980, pp. 1023-1028.

[66] Davies, R.G., "The Deformation Behavior of a Vanadium-Strengthened Dual Phase Steel", Metallurgical Transactions A, v. 9A, January 1978, pp. 41-52.

[67] Mileiko, S.T., "The Tensile Strength and Ductility of Continuous Fibre Composites", Journal of Materials Science, v. 4, 1969, pp. 974-977.

[68] Garmong, G. and Thompson, R.B., "A Theory for the Mechanical Properties of Metal-Matrix Composites at Ultimate Loading", Metallurgical Transactions, v. 4, March 1973, pp. 863-873.

[69] Ostrom, P., "Deformation Models for Two-Phase Materials", Metallurgical Transactions A, v. 12A, February 1981, pp. 355-357.

[70] Tomota, Y., Kuroki, K., Mori, T. and Tamura, I., "Tensile Deformation of Two-Ductile-Phase Alloys: Flow Curves of α-γ Fe-Cr-Ni Alloys", Materials Science and Engineering, 24, 1976, pp. 85-94.

[71] Pussegoda, L.N. and Tyson, W.R., "Modelling of a Dual-Phase Steel from its Constituents", Canadian Metallurgical Quarterly, v. 23, n. 3, 1984, pp. 341-347.

[72] Tamura, I., Tomota, Y. and Ozawa, M., "Strength and Ductility of Fe-Ni-C Alloys Composed of

Austenite and Martensite with Various Strength", International Conf. on the Strength of Metals and Alloys, Inst. Metals and Iron Steel Inst., 1973, pp. 611-615.

[73] Rios, P.R., Guimaraes, J.R.C. and Chawla, K.K., "Modelling of the Stress-Strain Curves of Dual Phase Steels", Scripta Metallurgica, v. 15, 1981, pp. 899-904.

[74] Goel, N.C., Sangal, S. and Tangri, K., "A Theoretical Model for the Flow Behavior of Commercial Dual-Phase Steels Containing Metastable Retained Austenite : Part I. Derivation of Flow Curve Equations", Metallurgical Transactions A, v. 16A, November 1985, pp. 2013-2021.

[75] Sangal, S., Goel, N.C. and Tangri, K., "A Theoretical Model for the Flow Behavior of Commercial Dual-Phase Steels Containing Metastable Retained Austenite : Part II. Calculation of Flow Curves", Metallurgical Transactions A, v. 16A, November 1985, pp. 2023-2029.

[76] Hill, R., "The Mathematical Theory of Plasticity", Oxford University Press, 1983.

[77] Johnson, W., Sowerby, R. and Haddow, J.B., "Plane-Strain Slip-Line Fields: Theory and Bibliography", New York : American Elsevier Publishing Co., Inc., 1970.

[78] Shield, R.T. and Drucker, D.C., "The Application of Limit Analysis to Punch-Indentation Problems", Trans. ASME, Journal of Applied Mechanics, December 1953, pp. 453-460.

[79] Sokolovsky, W.W., "The Theory of Plasticity - An Outline of Work Done in Russia", Trans. ASME, Journal of Applied Mechanics, v. 13, March 1946, pp. A1-A10.

[80] Dugdale, D.S., "Cone Indentation Experiments", Journal of the Mechanics and Physics of Solids, v. 2, 1954, pp. 265-277.

[81] Dugdale, D.S., "Experiments with Pyramidal Indenters - Part I", Journal of the Mechanics and Physics of Solids, v. 3, 1955, pp. 197-205.

[82] Dugdale, D.S., "Experiments with Pyramidal Indenters - Part II", Journal of the Mechanics and Physics of Solids, v. 3, 1955, pp. 206-211.

[83] Williams, G.H. and O'Neill, H., "The Straining of Metals by Indentation including Work-Softening Effects", Journal of the Iron and Steel Institute, v. 182, March 1956, pp. 266-273.

[84] Mulhearn, T.O., "The Deformation of Metals by Vickers-Type Pyramidal Indenters", Journal of the Mechanics and Physics of Solids, v. 7, 1959, pp. 85-96.

[85] Samuels, L.E. and Mulhearn, T.O., "An Experimental Investigation of the Deformed Zone Associated with Indentation Hardness Impressions", Journal of the Mechanics and Physics of Solids, v. 5, 1957, pp. 125-134.

[86] Lockett, F.J., "Indentation of a Rigid/Plastic Material by a Conical Indenter", Journal of the Mechanics and Physics of Solids, v. 11, 1963, pp. 345-355.

[87] Shaw, M.C. and DeSalvo, G.J., "A New Approach to Plasticity and Its Application to Blunt Indenters", Trans. ASME, Journal of Engineering for Industry, May 1970, pp. 469-479.

[88] Shaw, M.C. and DeSalvo, G.J., "On the Plastic Flow Beneath a Blunt Axisymmetric Indenter", Trans. ASME, Journal of Engineering for Industry, May 1970, pp. 480-494.

[89] Lee, C.H. and Kobayashi, S., "Elastoplastic Analysis of Plane-Strain and Axisymmetric Flat Punch Indentation by the Finite Element Method", Int. J. Mech. Sci., v. 12, 1970, pp. 349-370.

[90] Hardy, C., Baronet, N. and Tordion, G.V., "The Elasto-Plastic Indentation of a Half Space by a Rigid Sphere", Int. J. Numerical Methods in Engineering, v. 3, 1971, pp. 451-462.

[91] Yokouchi, Y., Chou, T.W. and Greenfield, I.G., "Elasto-Plastic Analysis of Indentation Damages in Copper: Work-Hardening and Residual Stress", Metallurgical Transactions A, v. 10A, November 1983, pp. 2415-2421.

[92] Valliappan, S., Lee, I.K. and Boonlualohr, P., "Non-Linear Analysis of Contact Problems", Numerical Methods in Coupled Systems, ed. R.W. Lewis, P. Bettess and E. Hinton, Toronto: John Wiley & Sons Ltd., chapter 8, 1984, pp. 231-253.

[93] Bhasin, Y.P., Oxley, P.L.B., and Roth, R.N., "An Experimentally-Determined Slip-Line Field for Plane-Strain Wedge Indentation of a Strain-Hardening Material", Journal of the Mechanics and Physics of Solids, v. 28, 1980, pp. 149-165.

[94] Johnson, W. and Mellor, P.B., "Engineering Plasticity", Chichester, England: Ellis Horwood Ltd., 1983.

[95] Shigley, J.E., "Mechanical Engineering Design", New York: McGraw-Hill, Inc., Third Edition, 1977.

[96] Morrow, J., Ross, A.S. and Sinclair, G.M., "Relaxation of Residual Stresses due to Fatigue Loading", SAE Transactions, v. 68, 1960, pp. 40-48.

[97] Morrow, J. and Sinclair, G.M., "Cycle-Dependent Stress Relaxation", Symposium on Basic Mechanisms of Fatigue, ASTM STP 237, 1958, pp. 83-109.

Appendix A

Elastic-Plastic Bending of a Beam

The magnitude and the distribution of residual stresses induced by surface rolling with one roller can be altered by bending if yielding occurs within the test specimen. Therefore, it is important to determine whether or not the HSLA steel and/or the dual phase steel specimens exhibited plastic deformation of the surface layer from bending produced by surface rolling with one roller.

The problem of elastic-plastic bending of a beam can be simplified by assuming that plane sections remain plane (Bernoulli-Navier assumption) and that the plastic zones are isotropic and extend homogeneously. It is also assumed that the material flows in an elastic-perfectly plastic manner [40-43].

From the circular cross-section beam shown in Figure A1, the statical moment of the stresses in the elastic-plastic state is:

$$M_i = 4 \int \sigma \, y \, dA + 4 \int \sigma_o \, y \, dA \quad . \qquad (A1)$$

Also, from Figure A1, the limits for the above integrals can be determined and then substituted into equation (A1) along with the equation defining the stress in the elastic portion of the cross-section;

$$\sigma = \frac{y}{y_o} \sigma_o \quad . \qquad (A2)$$

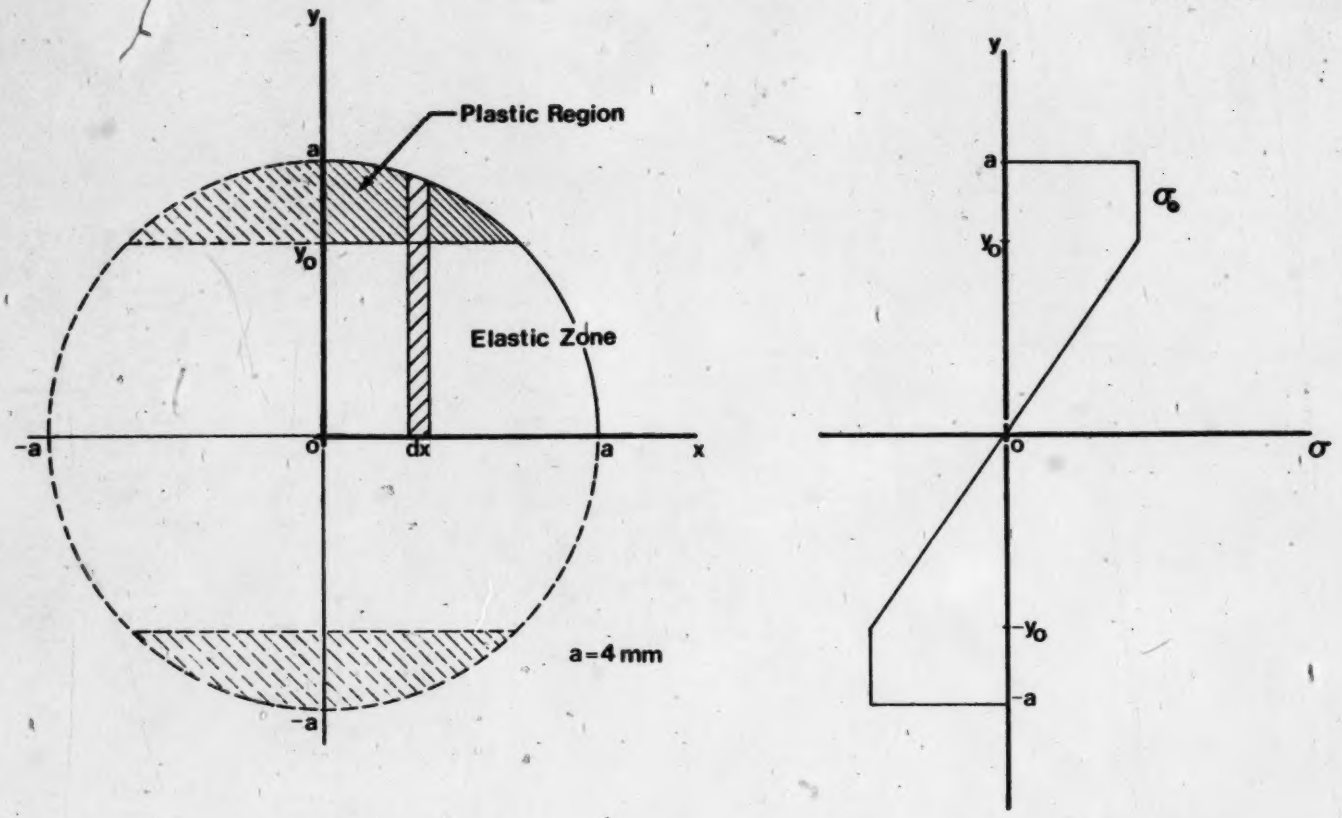

Figure A1 : Cross–Section and Stress Distribution of an Elastic–Plastic Circular Section in Bending.

And, the moment of the stresses is:

$$M_i = 4\left\{\int_0^{y_o}\left(\int_0^{\sqrt{a^2+y_o^2}}\left(\frac{y}{y_o}\sigma_o\right) y\,dx\right)dy + \int_{\sqrt{a^2+y_o^2}}^{a}\left(\int_0^{\sqrt{a^2+x^2}}\left(\frac{y}{y_o}\sigma_o\right) y\,dy\right)dx\right\} + 4\left\{\int_0^{\sqrt{a^2+y_o^2}}\left(\int_{y_o}^{\sqrt{a^2+x^2}}\sigma_o\, y\,dy\right)dx\right\} . \qquad (A3)$$

After integrating equation (A3), one obtains;

$$M_i = \frac{\sigma_o}{6}\left(1\tfrac{1}{2}a^2 - 2y_o^2\right)\sqrt{a^2 - y_o^2} + \frac{\sigma_o}{2}\frac{a^4}{y_o}\left[\frac{\pi}{2} + \cos^{-1}\left(\frac{y_o}{a}\right)\right] . \qquad (A4)$$

The depth of plastic deformation, $a - y_o$ can be determined by substituting into equation (A4) the moment calculated from the experimentally observed deflection of the test specimen. For the dual phase steel, the deflection was 0.064 mm (0.0025 in.) with a roller load of 178 N and a specimen diameter of approximately 8 mm. The bending moment corresponding to the deflection was 11.25 N·m.

Using a proportional limit of 215 MPa for the dual phase steel, the distance to the plastic zone from the bending axis, y_o is 3.999485 mm and the depth of the plastic zone is then $a - y_o$, 0.0005 mm. This corresponds to a tensile residual stress of approximately 9 MPa. Therefore, the surface of the dual phase test specimen has begun to yield in bending due to the applied pressure of one roller

during surface rolling.

Consequently, the large bending stresses will change the magnitude and distribution of the contact pressure residual stresses to some extent since the depth of penetration of surface rolling of the dual phase steel is about 0.57 mm.

The HSLA steel will not be affected by bending because of the high proportional limit which is approximately twice that of the dual phase steel.

Therefore, it was decided to use two rollers in the surface rolling procedure to halt the bending of the test specimen.

Appendix B

Fatigue Life Data

HSLA Steel :

Specimen Number	Applied Alternating Direct Stress (MPa)	(ksi)	Life (cycles)	Notes
Polished				
HSLA-1F	346.5	50.25	262420	
HSLA-2F	332.6	48.25	1010310	
HSLA-3F	318.8	46.25	1159140	
HSLA-4F	332.6	48.25	562270	
HSLA-5F	344.8	50.00	220130	
HSLA-6F	310.3	45.00	1195000	
HSLA-7F	299.9	43.50	2973600	
HSLA-8F	337.9	49.00	379800	
HSLA-9F	310.3	45.00	1279180	
HSLA-10F	317.2	46.00	983870	
HSLA-11F	296.5	43.00	9000000	No Failure
HSLA-12F	303.4	44.00	1182450	
HSLA-13F	303.4	44.00	1344820	
HSLA-14F	299.9	43.50	---	Grip Failure
HSLA-15F	337.9	49.00	503470	
Surface Rolled				
HSLA-1FDR	337.9	49.00	2197330	
HSLA-2FDR	344.8	50.00	2420760	
HSLA-3FDR	351.6	51.00	1174400	
HSLA-4FDR	358.5	52.00	---	Control Failure
HSLA-5FDR	365.4	53.00	---	Control Failure
HSLA-6FDR	358.5	52.00	761320	
HSLA-7FDR	362.0	52.50	1294890	
HSLA-8FDR	337.9	49.00	4203090	Thread Failure
HSLA-9FDR	372.3	54.00	451060	
HSLA-10FDR	351.6	51.00	1149980	

Dual Phase Steel :

Specimen Number	Applied Alternating Direct Stress (MPa)	(ksi)	Life (cycles)	Notes
Polished				
DP-1F	268.9	40.00	3922140	Thread Failure
DP-2F	268.9	40.00	2966210	Thread Failure
DP-3F	289.6	42.00	---	Grip Failure
DP-4F	289.6	42.00	182270	
DP-5F	286.1	41.50	181820	
DP-6F	282.7	41.00	254320	
Surface Rolled				
DP-1FDR	282.7	41.00	3438960	
DP-2FDR	303.4	44.00	100130	
DP-3FDR	296.5	43.00	899160	
DP-4FDR	289.6	42.00	---	Control Failure
DP-5FDR	286.1	41.50	4635320	Thread Failure
DP-6FDR	299.9	43.50	455760	
DP-7FDR	293.0	42.50	389000	
DP-8FDR	289.6	42.00	2405100	Thread Failure
Surface Rolled, Aged at 180°C for 30 min.				
DP-1FDRA	319.9	46.40	228110	